Stellenbosch
UNIVERSITY
IYUNIVESITHI
UNIVERSITEIT

forward together
sonke siya phambili
saam vorentoe

CAF Central Analytical Facilities
STELLENBOSCH UNIVERSITY

2021/2022 Annual Report *of the* Central Analytical Facilities

Characterisation of melanophores in lizard skin - p 16

2022 CAF committee:

Vice-Rector Research and DRD
Prof Eugene Cloete
Dr Therina Theron
Ms Malene Fouché (Secretariat)

CAF Management
Prof Gary Stevens (Director)

Deans and Vice-Deans
Prof Danie Brink (Dean Faculty of AgriScience)
Prof Gey van Pittius (Vice-Dean Research Faculty of Medicine and Health Sciences & Subcommittee C)
Prof Petrie Meyer (Vice-Dean Research Faculty of Engineering)
Prof Louise Warnich (Dean Faculty of Science)

Subcommittee B
Prof KJ Esler

PIs on recent equipment grant applications
Prof Johan Burger
Prof Bert Klumperman
Dr Ben Loos
Prof Quinette Louw
Prof Marena Manley
Prof Kathy Myburgh
Prof Marina Rautenbach
Prof Gerhard Walzl
Prof James Warwick
Prof André van der Merwe

Chair of the BIOGRIP Node steering committee
Dr Suzanne Grenfell

Invited CAF Unit Managers and DSI-funded Node Directors
Dr Marietjie Stander
Mr Carel van Heerden
Dr Janine Colling
Ms Fransien Kamper
Dr Alex Doruyter

www.sun.ac.za/caf

Contents

Overview

In 2022 CAF is projected to once again realise a small profit, the first time in four years that this has been the case. As illustrated by Figure 1, CAF lost a significant amount of money in 2019, principally due to changes in the way the NRF handled post-graduate bursaries. Then demand for services was heavily affected by the pandemic in 2020 and 2021, with a successful claim against interruption of business insurance thankfully shielding CAF from the worst financial effects. The value of services delivered in 2022 is projected to be just slightly higher than 2019 values, indicating that demand for services is still some considerable way the trend defined by the pre-pandemic years. Consequently, CAF may well have a stronger than predicted 2nd half of 2022, as recovery gathers pace due to the resumption of normal research activities.

The profit and loss graphs for the CAF units presented in Figure 2 highlights a long-standing financial reality for CAF operations. This is that only the Mass Spectrometry unit makes a significant income, which helps offset the losses by some other units. The 2022 picture is considerably better than that of 2021 because resignations of senor staff in the CT unit and the Neuromechanics unit have resulted in significant savings in both areas. Additionally, the resumption of services at the NMR unit, after the refurbishment of the labs and the installation of the new NMR spectrometers, has resulted in a substantially better outlook for the unit, while the improvement at the DNA unit is principally due to normalization of demand.

Figure 2 also reflects structural changed aimed improving CAF cost-effectiveness in the long term. The Scanning Electron Microscopy (SEM) unit, has become the Microscopy unit by incorporating the relevant staff and equipment involved in light microscopy from the former Fluorescent Microscopy (FM) unit, which has
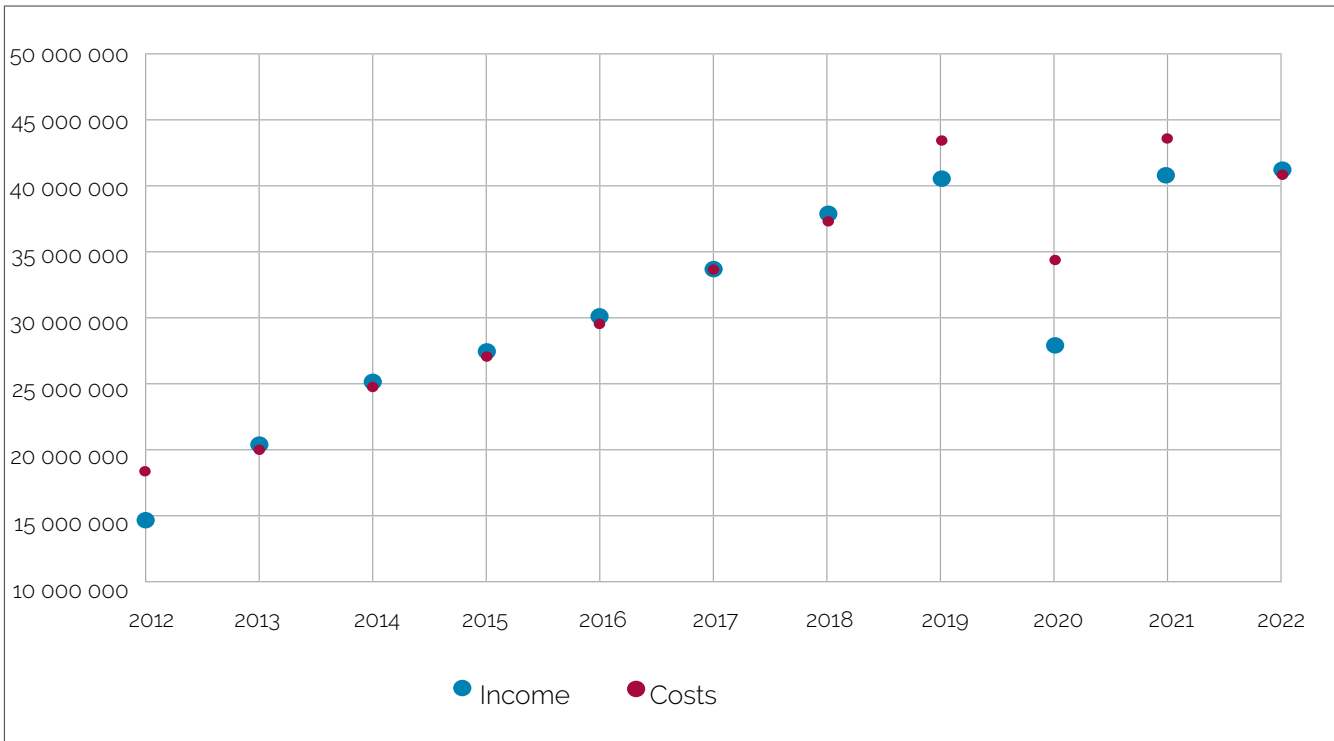
Figure 1: *CAF income and costs for the period 2012 to 2022. A significant component of CAF cost is related to the purchase of expensive reagents. This component of cost scales with demand and explains the significant decrease in cost during 2020 when the COVID pandemic had the greatest impact on the volume of work flowing through CAF labs. It is important that CAF takes the steps during 2022 to reestablish the sustainable growth in services that is apparent in the information for 2013 to 2018.*
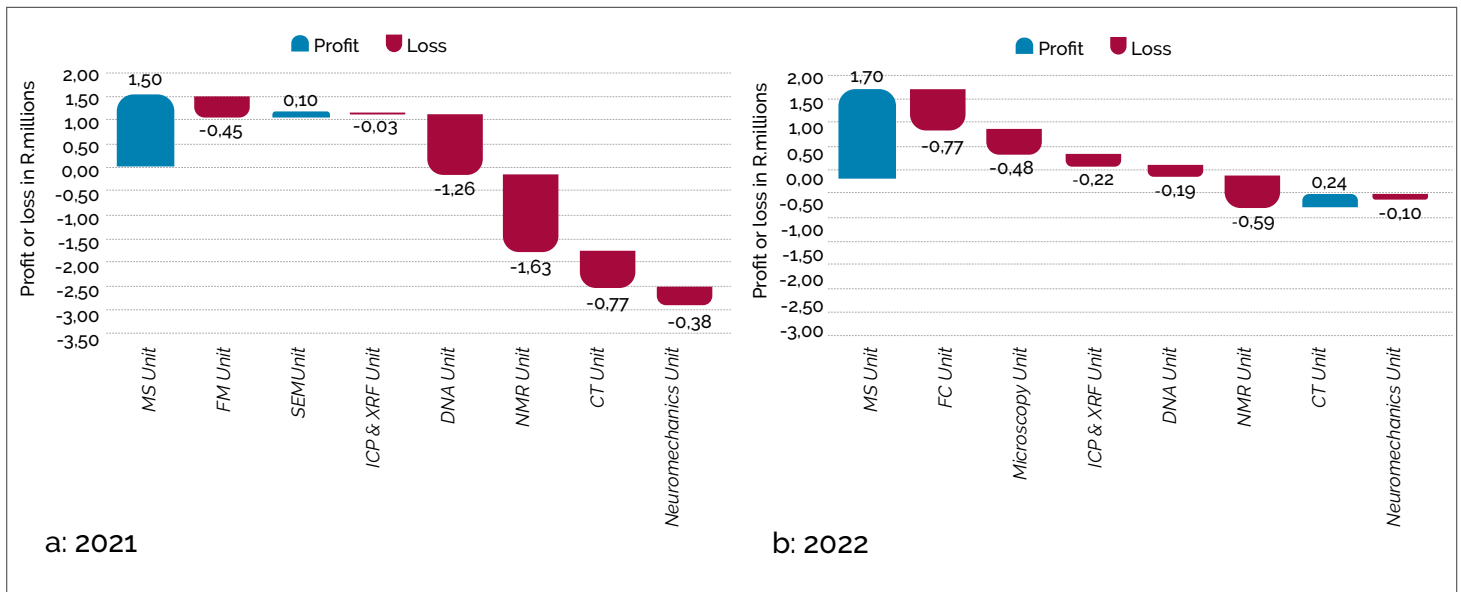
Figure 2: *Profit and loss amongst CAF units in a) 2021 and b) 2022. Only direct income to the units is portrayed.*

become the Flow Cytometry (FC) unit, so flow cytometry has been separated from microscopy, allowing both sets of staff to focus on a specific analytical function.

In the CAF report of 2020/21 the growing need for renewal of the CAF equipment base was highlighted. There will be a National Equipment Program competitive grant round in 2022 and applications will be submitted for two items to be hosted within CAF. One of these is a high content imaging confocal microscope and the other is a high resolution ion-mobility mass spectrometer. Both applications are very important to research at SU, but the mass spectrometry application for R19 million, is critically important to the financial stability of CAF because it will replace aging equipment at the Mass Spectrometry unit, without which the unit would not be able to deliver a profit.

In closing this introduction to the 2021/22 CAF report it is important to note that this is the last report that will serve during Prof Eugene Cloete's term as Deputy Vice Chancellor for Research at Stellenbosch University. Eugene, I would like to thank you personally, and on behalf of all CAF staff, for the tremendous support and guidance you have provided over the years. We wish you all the very best for the future.

Prof Gary Stevens
CAF Director

Profile of the CAF client base

Since 2017, CAF has collected comprehensive information on the use of CAF facilities. This enables us to provide the NRF with a comprehensive profile of the use of NEP-funded equipment. Figures 3 - 7 below provide some information on the CAF client base in 2021 as well as on possible changes to the profile of CAF clients over time:

Figure 3: *The number of active CAF clients from 2017 to 2021, including the percentage of industry and academic clients.*
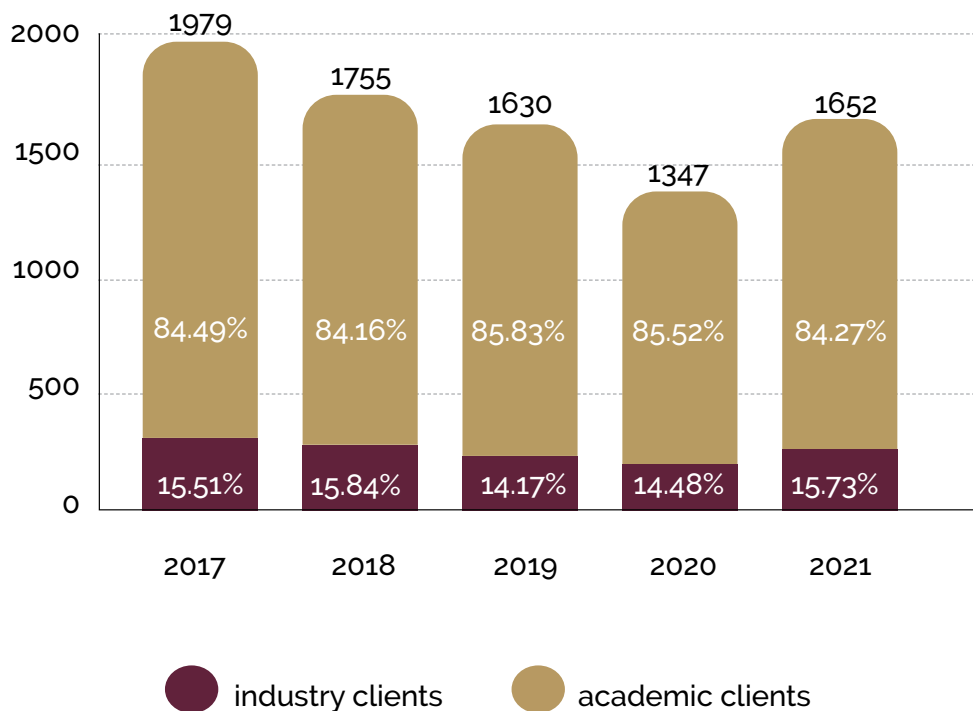
Figure 4: *The subdivision of CAF academic clients according to type of institution for 2021.*

- Foreign universities 42
- Other RSA universities 474
- Other RSA research institutions 70
- Stellenbosch University 807
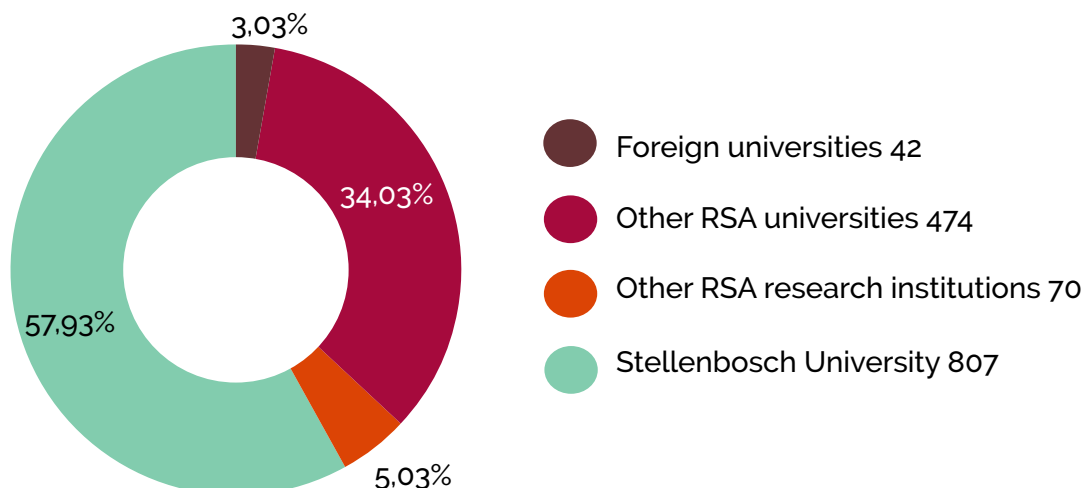
Figure 5: *The profile of CAF academic clients for 2021.*

Students 877 — 62,81%
Researchers 516 — 37,19%
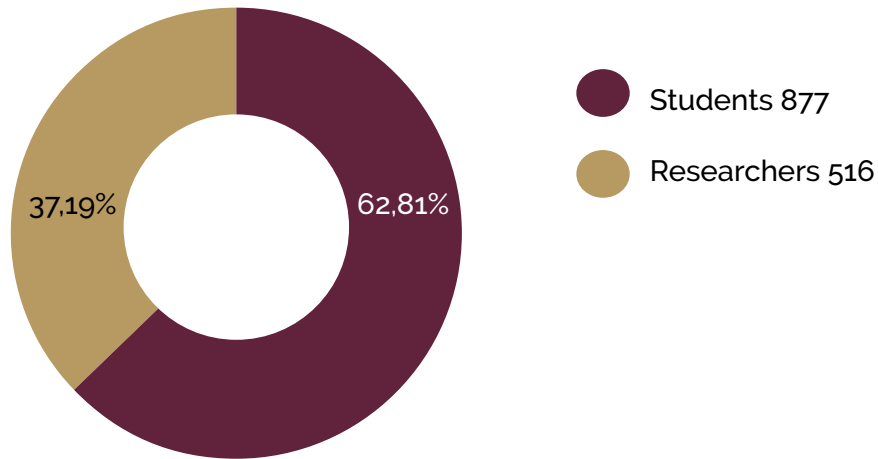
Figure 6: *The subdivision according to level of study of the 62,81% students for 2021 compared with 2020 and 2019.*

	Honours	Masters	PhD	Undergraduate	Not indicated
2019	140	377	332	37	40
2020	101	336	299	16	
2021	99	376	335	27	
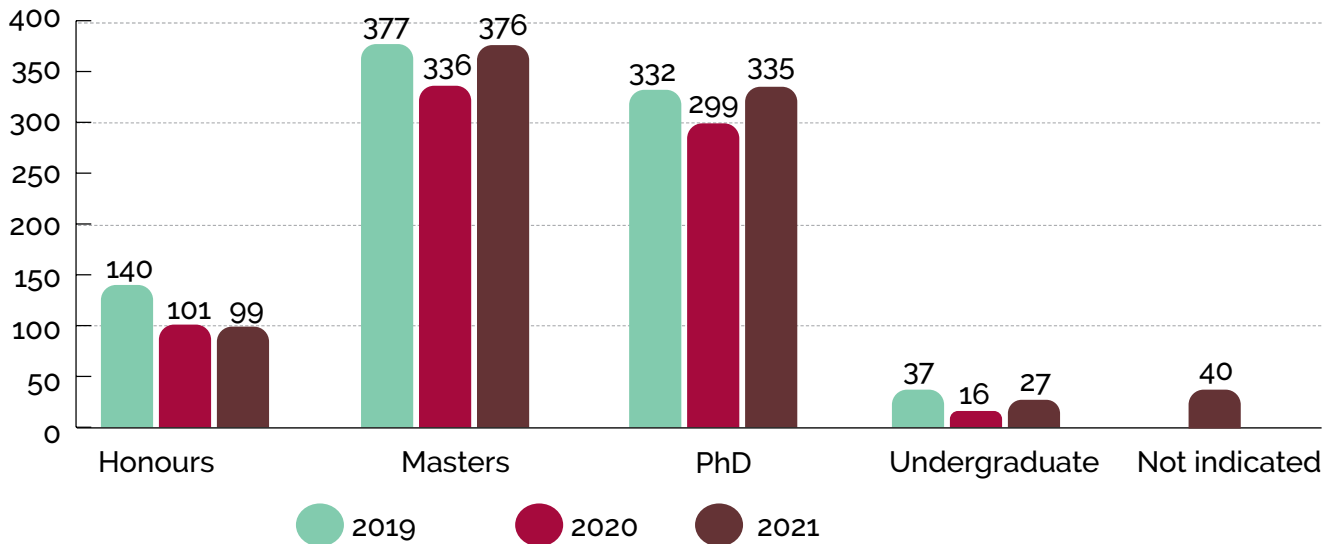
Figure 7: *Stellenbosch University student clients of CAF for 2021 classified according to faculty.*

Faculty of Agrisciences 195 — 24,16%
Faculty of Engineering 105 — 13%
Faculty of Medicine & Health Sciences 153 — 18,96%
Faculty of Science 350 — 43,38%
Faculty Art & Social Sciences 4 — 0,5%
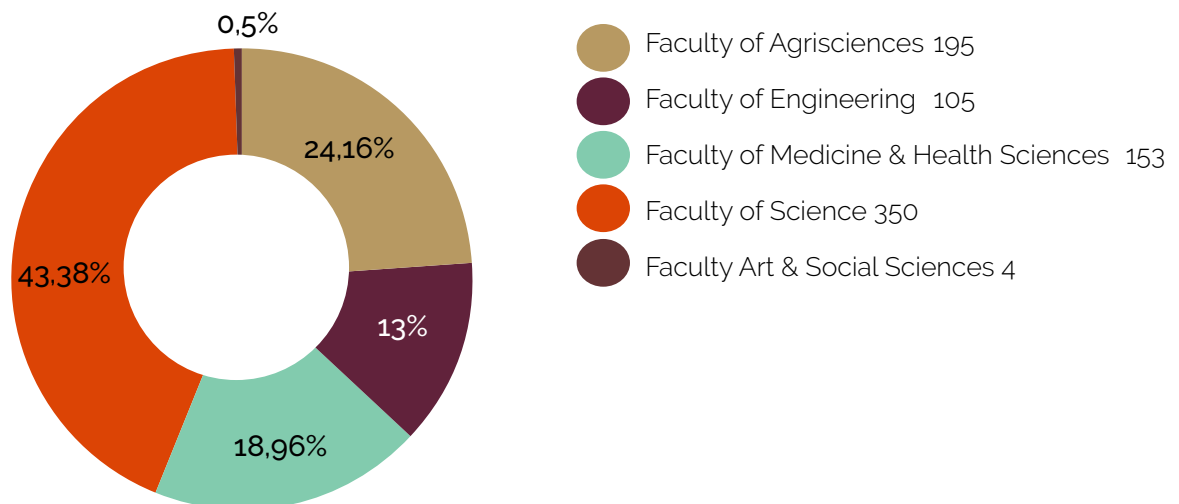
Unravelling the potential of a novel therapeutic agent for the treatment of Alzheimer's disease by pushing the limits of microscopy

By Lize Engelbrecht

With the use of advanced microscopy techniques, researchers were able to show how a natural polyamine, spermidine, could enhance treatment strategies against neurodegeneration associated with Alzheimer's disease.

During her PhD, Dr Dumisile Lumkwana, also a former analyst at CAF Fluorescence Microscopy Unit, made use of superresolution microscopy and correlative light and electron microscopy (CLEM) to study the effects of spermidine in neuronal cells in which Alzheimer's-related effects had been induced. This work was recently published in the journal *Frontiers in Cell and Developmental Biology* (*DOI:10.3389/ fcell.2022.819571*).

Models for Alzheimer's disease

During Alzheimer's disease, certain proteins accumulate and aggregate in neuronal cells, causing neurotoxicity. One such protein is amyloid precursor protein (APP), which in turn leads to the generation of the aggregate-prone peptide amyloid-beta. Using cells genetically modified to produce excessive levels of APP and amyloid-beta, its accumulation mimics the protein accumulation associated with Alzheimer's disease. Some environmental pollutants and agricultural pesticides, such as paraquat, are neurotoxic and have also been associated with neurodegenerative disease.

Under supervision of Prof Ben Loos from the Department of Physiological Sciences, Dr Lumkwana investigated the efficacy of spermidine 1) in cells overexpressing APP, 2) in cells treated with paraquat and 3) in a mouse model where neuronal damage had been induced by paraquat administration.

Cellular viability was reduced over time in mutant neuronal cells overexpressing APP, while spermidine improved the cellular viability over time significantly. Using flow cytometry, performed by Dr Rozanne Adams, it was also shown that paraquat reduced neuronal cell viability and induced a significant increase in production of reactive oxygen species (ROS) in the cells. Both low and high concentrations of spermidine improved cell viability significantly, but ROS production was only reduced when a low concentration of spermidine was used, suggesting that the effects of spermidine is concentration dependent and should be investigated accordingly. These results showed that the use of both APP overexpressing cells and cells exposed to paraquat toxicity was ideal to study the mechanisms through which spermidine could provide protection against neurodegeneration.

Targeting the cellular clean-up process

One such mechanism of action could be through the cellular process called autophagy, which is responsible for removing protein aggregates, toxic agents and other damaged cell content. During autophagy, cargo collects in vacuoles in the cell and is subsequently taken through a process of degradation. First, molecules are collected in a phagophore, which then develops into an autophagosome and eventually fuses with a lysosome to form what is called an autolysosome, where pH-dependent degradation takes place. The rate of protein degradation through the process is called the autophagic flux, and an increased autophagic flux could be beneficial, especially since autophagy activity has been shown to decline during ageing. Increasing autophagy activity is the focus of many studies to find improved treatment strategies against neurodegenerative diseases, especially those related to ageing.

Assessing the autophagic flux

The LSM780 confocal microscope with ELYRA PS1 superresolution platforms in the CAF Microscopy Unit (previously Fluorescence Microscopy Unit) was used to visualise a key component of matured autophagosomes, namely microtubule-associated protein-1 light chain or LC3 protein. This protein can be used to measure various parameters of the autophagic flux. Here, a labelling strategy whereby LC3 presented yellow in autophagosomes and red in autolysosomes with confocal microscopy revealed that spermidine treatment at high (10 µM) and low (1 µM) concentrations significantly increased the number of autolysosomes but only high concentrations of spermidine increased the number of autophagosomes (Fig.8). The turnover time of the whole autophagic pool was reduced from 2 h in control cells to 0.64 h in the low-concentration treatment group and to 1.21 h in the high-concentration treatment group. These results suggest that there is a concentration-dependent increase in the autophagic flux in response to spermidine.

Correlative microscopy to study the autophagic vacuoles

Using transmission electron microscopy, which provides superior resolution to confocal microscopy, autophagic vacuole sizes were measured and found to be reduced in spermidine treatment groups. However, with electron microscopy, autophagosomes and autolysosomes are indistinguishable (hence referred to only as autophagic vacuoles), which prevents accurate analysis of changes in vacuolar size in the context of the autophagic flux. To distinguish autophagosomes from autolysosomes in the 3D cellular ultrastructure, a CLEM workflow had to be implemented. Structured illumination microscopy (SIM), which improves the resolution of fluorescence imaging, was first used to localise the autophagosomes. At the time of this study, 3D electron microscopy was not available at Stellenbosch University, so samples were fixed, prepared for electron microscopy and then sent to the Electron Microscopy Laboratory in the Science Technology Platform of the Francis Crick Institute in London for acquisition of electron microscopy micrographs in 3D on a focused-ion-beam scanning electron microscope (FIB-SEM). The research team of Prof Loos then used the superresolution microscopy results obtained in CAF to localise specifically the autophagosomes
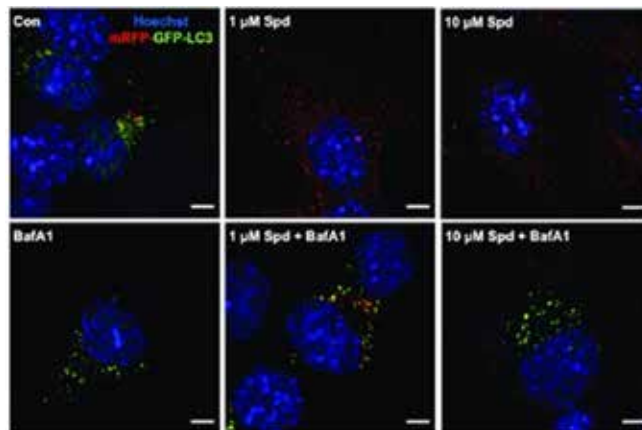
Figure 8: *A labelling strategy whereby LC3 presented yellow in autophagosomes and red in autolysosomes with confocal microscopy revealed that spermidine treatment at high (10 µM) and low (1 µM) concentrations significantly increased the number of autolysosomes but only high concentrations of spermidine increased the number of autophagosomes.*
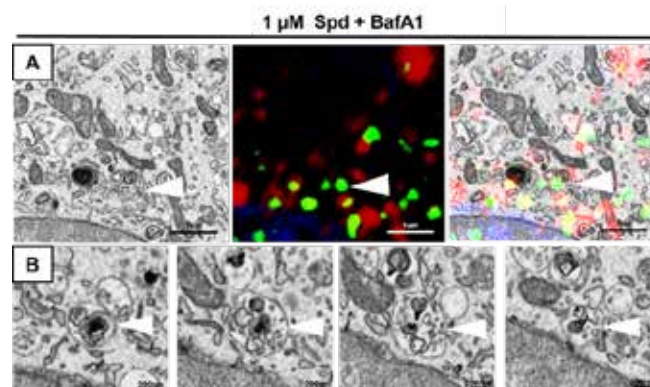
Figure 9: *The research team of Prof Loos used the superresolution microscopy results obtained in CAF to localise specifically the autophagosomes in the electron micrographs obtained in the United Kingdom.*
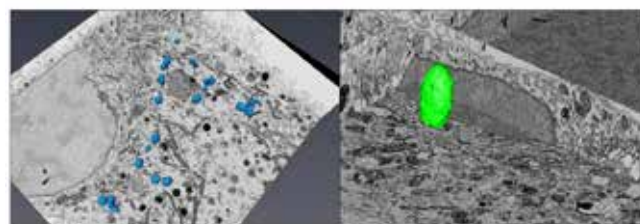
Figure 10: *After localisation, the autophagosomes had to be manually segmented through the entire stack of electron microscopy images to provide a 3D model of the autophagosomes in their entire volume before morphometric analysis could be performed.*

in the electron micrographs obtained in the United Kingdom (Fig. 9). After localisation, the autophagosomes had to be manually segmented through the entire stack of electron microscopy images to provide a 3D model of the autophagosomes in their entire volume before morphometric analysis could be performed (Fig. 10). One of the main role players in this process of correlation, segmentation and analysis was Dr Jurgen Kriel, who is now the operator of the ThermoFisher VolumeScope SEM at Tygerberg Medical Campus, but Nicola Heathcote, at the time an honours student and now a PhD student in the Loos lab, also played an important role.

Figure 11: *Using both superresolution microscopy platforms, namely SIM and stochastic optical reconstruction microscopy (STORM), on the neuronal cell models, it was observed that tubulin signal and density increased in paraquat-affected cells treated with spermidine.*

The results of CLEM revealed that spermidine played a significant role in size regulation of the autophagosomes, which is related to effective cargo clearance. The volume and surface area of autophagosomes were increased in the low-concentration treated cells, while these parameters were reduced in the high-concentration treatment group. These results confirmed the concentration-dependent effect of spermidine, which deserves further study, and further highlighted the requirement for high-precision identification of cellular organelles in electron micrographs through the identification strategies made possible with fluorescence methods and subsequent correlation.

Effects of spermidine on the cellular transport proteins

Autophagosome transport relies on the transport systems of the cell to accommodate association with lysosomes for fusion. Tubulin, especially in an acetylated state, is one of the scaffold proteins providing a transport mode for organelles such as autophagosomes and is structurally most effectively studied with superresolution techniques due to its fine structure. Using both superresolution microscopy platforms, namely SIM and stochastic optical reconstruction microscopy (STORM), on the neuronal cell models, it was observed that tubulin signal and density increased in paraquat-affected cells treated with spermidine (Fig. 11). However, from measurements in mouse brains, it seemed

that the effects of spermidine and paraquat treatments on acetylated tubulin levels were region specific. The localisation and structure of acetylated tubulin were not determined in the tissue samples, but the results obtained in the cells are motivation for further study on the effects of spermidine on transport proteins in live models.

Accurate measurements of amyloid precursor protein accumulation and clearance

Visualisation and accurate quantification of protein accumulation and clearance provide strong evidence of the efficacy of therapeutic drugs for neurodegenerative diseases. Here, the STORM superresolution method was used to determine the number of APP aggregates as well as their relative sizes. With conventional confocal microscopy, structures smaller than 200 nm cannot be measured accurately, while SIM allows only accurate measurements down to 100 nm. With STORM, resolution can be improved to several nanometres. For this method, samples are usually visualised in a buffer that allows the fluorescence molecules to blink rather than constantly emit their fluorescence together with neighbouring fluorophores. The blinking effect enables the researcher, through software algorithms, to localise the single fluorescence molecules used for protein labelling to subresolution precision and to reconstitute the fluorescence image from the map of localised fluorophores instead of their actual emission.
APP overexpression was induced by administration of butyric acid (BA) for 24 h and 48 h

respectively. APP clusters ranged from 6 to 50 nm2, with an abundance of APP clusters from 6 to 10 nm2 at 24 h. The number of APP clusters at the 48-h timepoint was significantly increased for all sizes. In the presence of spermidine, clearance of APP clusters was evident, especially in the reduced number of clusters 6-25 nm2 at the 24-h timepoint, while APP cluster clearance of all sizes was evident at 48 h (Fig.12). This study clearly shows visually how treatment with spermidine reduces protein accumulation and mediates clearance of such aggregates, revealing its potential in the treatment and prevention of diseases such as Alzheimer's disease.

Advanced microscopy techniques available for all

The correlative work of Dr Lumkwana was the forerunner for the acquisition of ThermoFisher Apreo Volumescope SEM for Stellenbosch University. Now housed by the CAF at the Tygerberg Medical Campus, the Volumescope is operated by Dr Kriel who collaborates closely with the team of the Electron Microscopy Laboratory of the Francis Crick Institute to ensure that methods are adequately implemented here. The availability of volumetric electron microscopy at Stellenbosch University opens opportunities for researchers in South Africa to study subcellular structure at much higher precision than what was previously possible. In another article in this report, Dr Kriel explains the power of 3D electron microscopy further.

The application of superresolution techniques has not been adopted in South Africa to the same extent as in areas such as Europe and the United States of America. While SIM does not require specialised sample preparation, only optimal signal from fluorescent markers, STORM requires an optimised environment for the fluorophores to blink. This has proven to be quite challenging, limiting the use of STORM. This study showcases how superresolution microscopy, in correlation with electron microscopy, can not only reveal novel information but also provide a means for structural measurements of much higher precision than confocal microscopy.
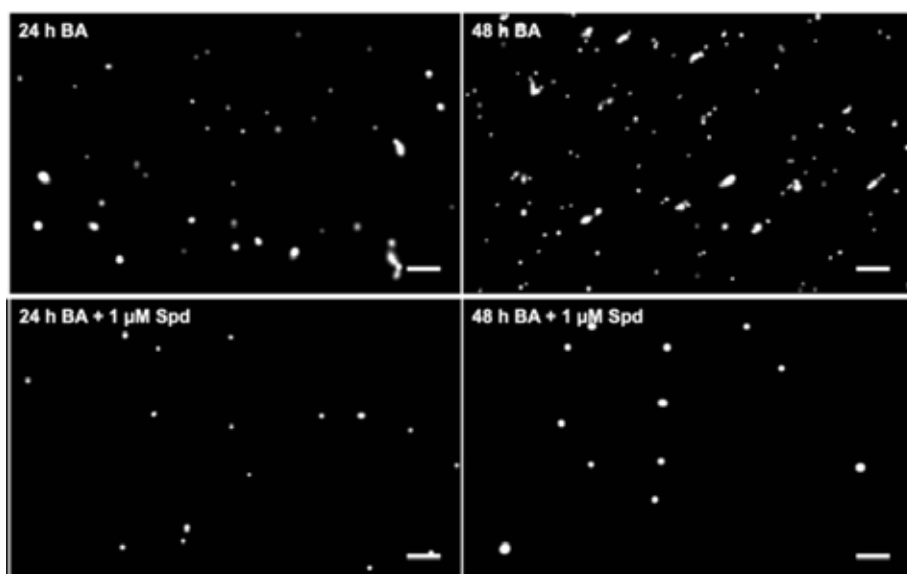
Figure 12: *The number of APP clusters at the 48-h timepoint was significantly increased for all sizes. In the presence of spermidine, clearance of APP clusters was evident, especially in the reduced number of clusters 6-25 nm^2 at the 24-h timepoint, while APP cluster clearance of all sizes was evident at 48h.*

Gold fingerprinting using laser ablation inductively coupled plasma mass spectrometry

By Riana Rossouw

Gold fingerprinting is the identification of different origins of gold through specific element associations, resulting in a characteristic chemical signature. Fingerprinting is used to distinguish between the geological sources of gold, for example lode versus alluvial gold, as well as to determine its geographical origin, with Colombian gold, for example, enriched in Pt and Brazilian gold higher in Pd. Fingerprinting is also an essential tool in the global battle against illicit precious metals trafficking, with the source of the illegally mined gold as well as the elements associated with the different extraction processes providing a unique signature.

Tracing illicitly mined gold

The illicit trafficking in precious metals creates a market of billions of USD per year, threatening global economies. Along with the impact on precious metal producers through theft, communities are also affected by the growing corruption, violence, and health and safety issues surrounding illicit mining activities. The challenge to law enforcement is proving that any seized material has been stolen. The value of fingerprinting therefore lies in the chemical characterisation of the seized material and comparing it against a reference databank containing fingerprint information of gold, either natural or processed. This databank is unfortunately not yet very extensive but is continually updated due to new legislation.

The elements of interest in fingerprint studies typically include As, Bi, Cr, V, Cu, Fe, Mn, Ni, Pb,

Pd, Sn, Zn, Ag, Cd, Rh, Ru, Sb, W and Hg. Except for Cu and Ag, most element concentrations vary at the ppm or lower levels. Laser ablation inductively coupled plasma mass spectrometry (LA ICP-MS) has long been used as the preferred analytical tool in fingerprint studies for several reasons:

- ICP-MS instruments have detection limits in the ppb range, enabling a large number of elements to be measured in a short time.
- Minimal destruction of samples that are small or precious occurs, with spot sizes typically ranging from 15 to 100 µm.
- Minimal sample preparation is required: Au grains or metal shavings are resin mounted and polished (Fig. 13).
- Analysis of Pb isotopes is useful to further distinguish gold provenance using laser ablation triple quadrupole ICP-MS, whereby ^{204}Hg interference on ^{204}Pb can be removed.

Figure. 13: *Resin-mounted gold shavings and grains placed in the laser ablation sample cell.*

Laser ablation method development

Since 2019, the LA ICP-MS Laboratory has been collaborating with an institution in Colombia to analyse samples from various sources within the country, including alluvial gold, gold seized from illegal mining activities and gold extracted through different process in order to identify fingerprinting
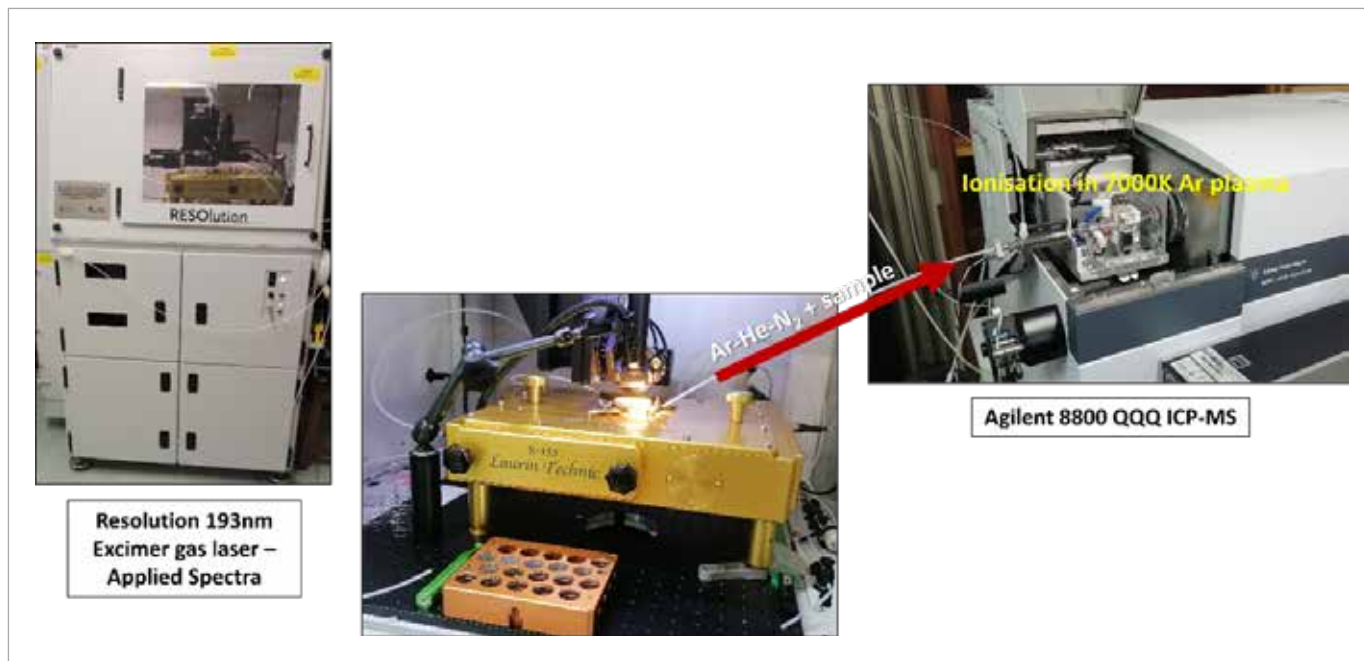
Figure 14: *Laser ablation QQQ ICP-MS setup*

elements unique to their environment as well as to optimise the analytical method. The equipment available at CAF includes an Applied Spectra Resolution 193 nm excimer laser connected to an Agilent 8800 triple quadrupole (QQQ) ICP-MS (Fig. 14).

There were several objectives in the method setup in order to obtain quantitative and reproducible results from gold material:

- A challenge in LA ICP-MS is the availability of matrix-matched standards required for quantitative analysis. National Institute of Standards and Technology (NIST) glass reference materials are the most common calibration standards, but their ablation properties are completely different from gold (Fig. 15), with more gold material volatilised compared to the NIST glass under the same conditions, resulting in higher reported concentrations for the elements in the gold sample. Gold matrix standards spiked with all the trace elements of interest are scarce and very expensive, but a custom standard was
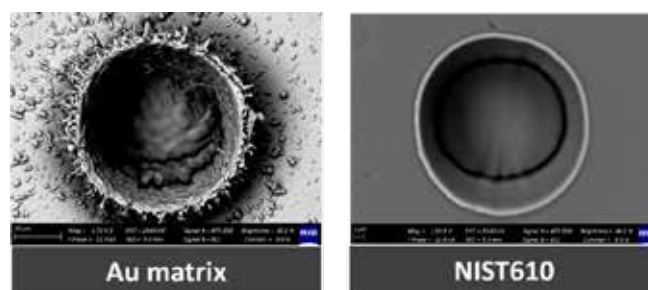
Figure 15: *Given the same laser settings, a gold matrix ablates completely different from a glass reference material, resulting in a larger volume of material transported to the ICP-MS so that element concentrations are typically overestimated.*

procured from Rand Refinery (Pty) Ltd South Africa, with elements distributed homogeneously at least at the 60 μm scale.
- The resolution of sample homogeneity had to be identified by a separate technique such as scanning electron microscopy (SEM) as it affects the major element composition used for LA ICP-MS quantification (Fig. 16) and determines the spot size (Fig. 17) and number of replicates for representative analysis (Fig. 18).
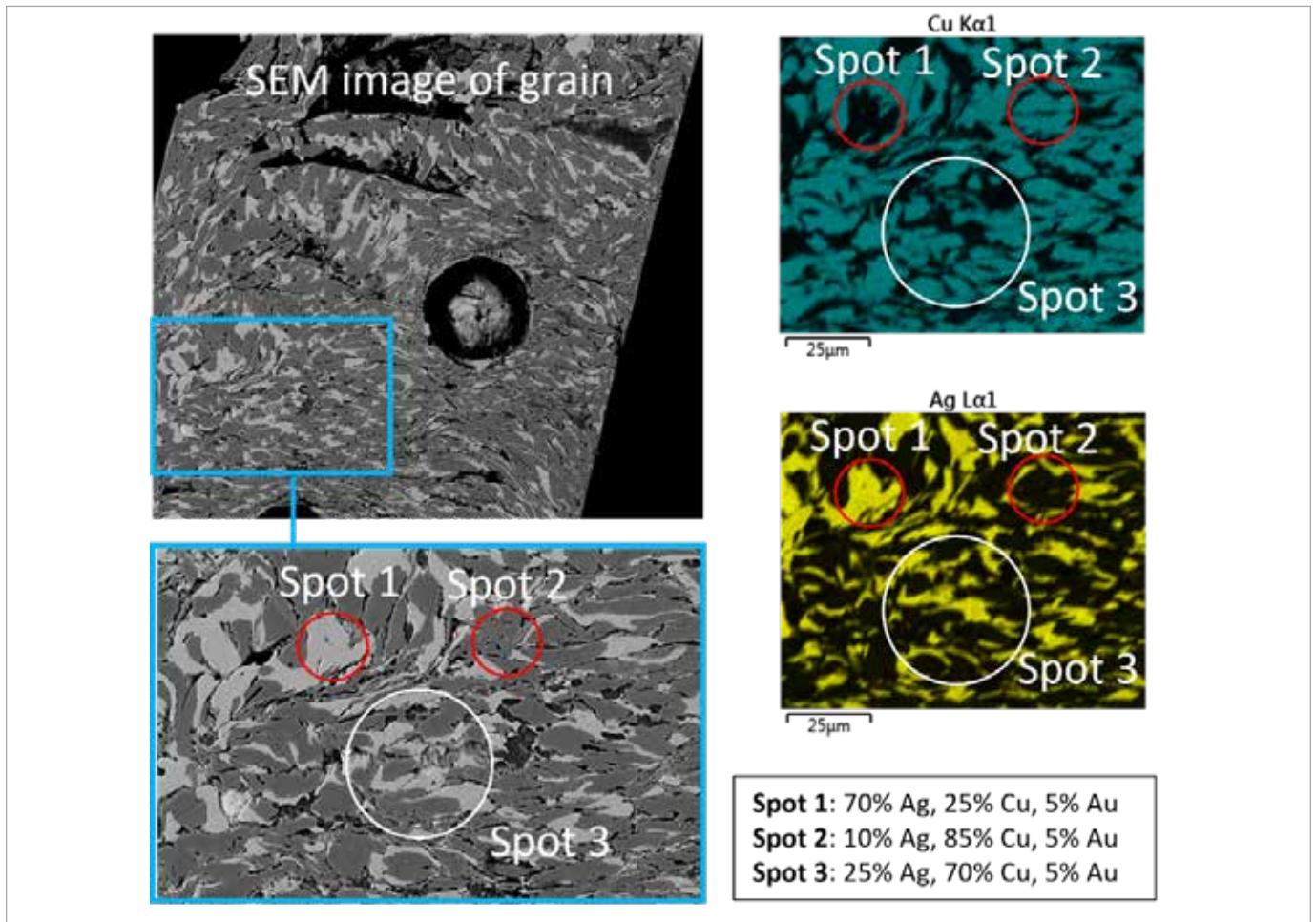
Figure 16: *SEM CL image of a gold grain showing fine-grained inhomogeneity in a Au-Ag-Cu alloy. If this sample was analysed with 20 μm spots at locations 1 and 2, the results would be completely different compared to a more averaged result ablating at a larger spot size of ~ 45 μm at location 3.*
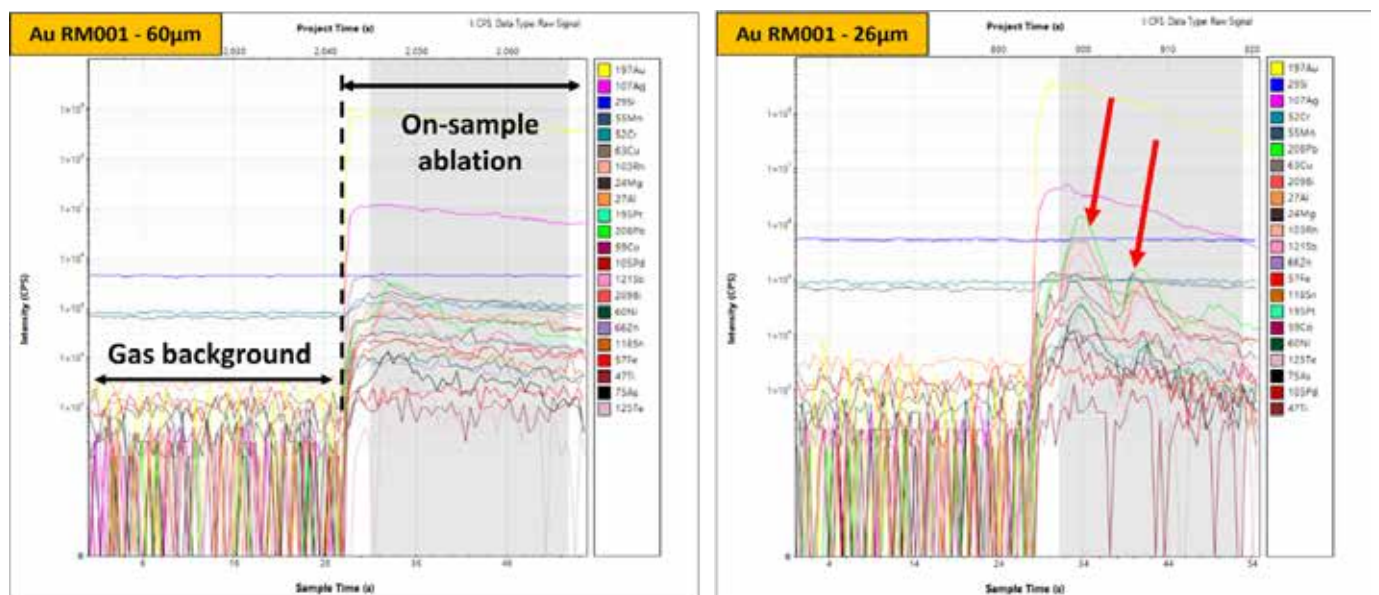
Figure 17: *At the larger spot size of 60 μm, a more representative area is sampled compared to the laser setting at 26 μm.*
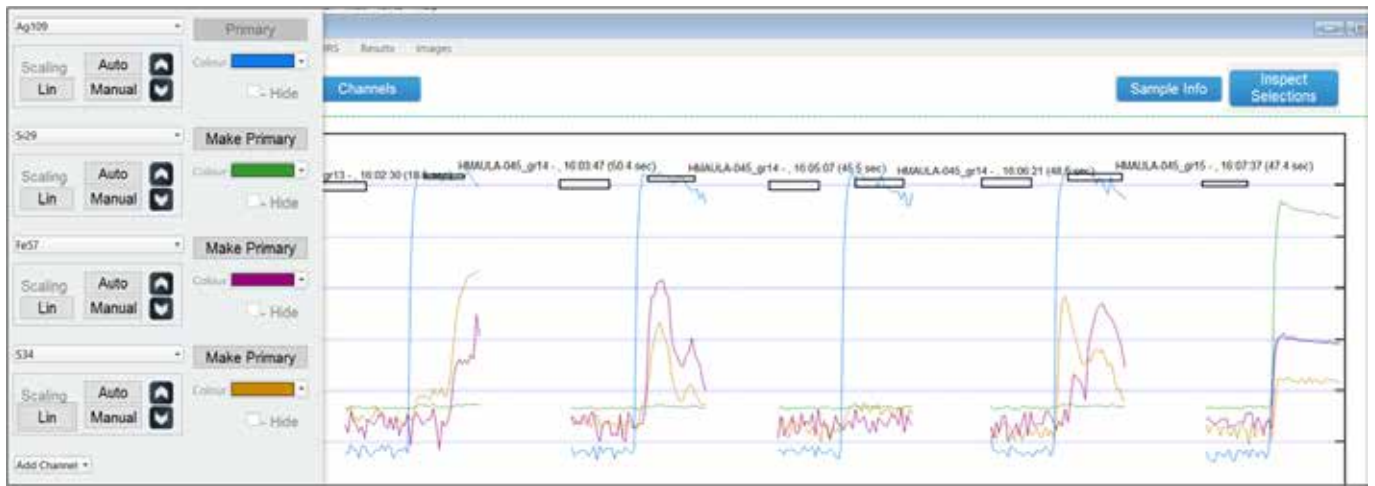
Figure 18: *Small inclusions could be present within the gold, with four replicates on the same material not yielding the same result. These inclusions can be averaged with the bulk of the analysis, excluded or quantified separately, depending on the nature of the gold.*
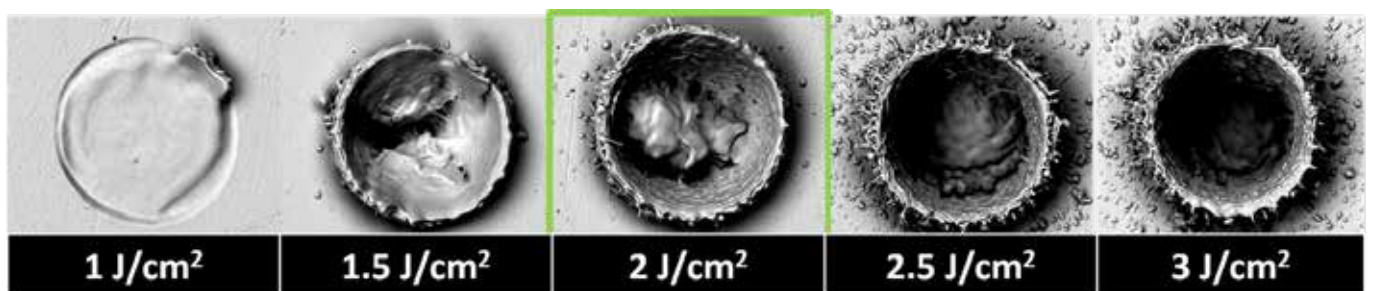
Figure 19: *Optimal laser parameters for gold ablation*

- Laser parameters were optimised to ablate the gold material with enough energy to volatilise the gold but not too high to cause excessive sputtering and generating ablated material of varying size fractions (Fig. 19).

The analytical method developed for the ongoing Colombian study can also be used in the chemical characterisation of gold from various geological environments and unravelling its formation history.

Proteomics analyses used to investigate long COVID

By Dr Maré Vlok

The SARS-CoV-2 virus called COVID-19 has paralysed the world since December 2019, and it was the scientific community that responded with treatment plans and accelerated vaccine development to treat and prevent this infection. Unfortunately, for some it became clear that SARS-CoV-2 infection could also have long-term effects. This lingering effect was first termed post-acute sequelae of COVID-19 (PASC) but is now commonly referred to as 'long COVID'.

Prof Etheresia Pretorius (Stellenbosch University) was one of the first scientists to investigate this phenomenon, and she contacted the CAF Proteomics Unit to assist.

One feature of plasma obtained from long COVID patients is the formation of micro-clots. However, this feature is not unique to long COVID but is also observed in diabetes sufferers, although the clinical picture is vastly different. Up to this point, proteomic analyses have used either clarified plasma or fully denatured and solubilised plasma proteins and have been unable to distinguish between proteins associated in clots and soluble proteins. We derived a strategy using a two-step digestion to isolate the clots. The first, under nondenaturing conditions, fragmented the soluble proteins, which were removed after centrifugation, and the second used nondenaturing conditions to break up the protein aggregates prior to trypsin digestion. After this step, it became apparent why the diabetes and long COVID clinical profiles were so different. The clots from diabetes patients were cleared after the first digestion whereas long COVID patients had clots resistant to the first trypsinisation step.
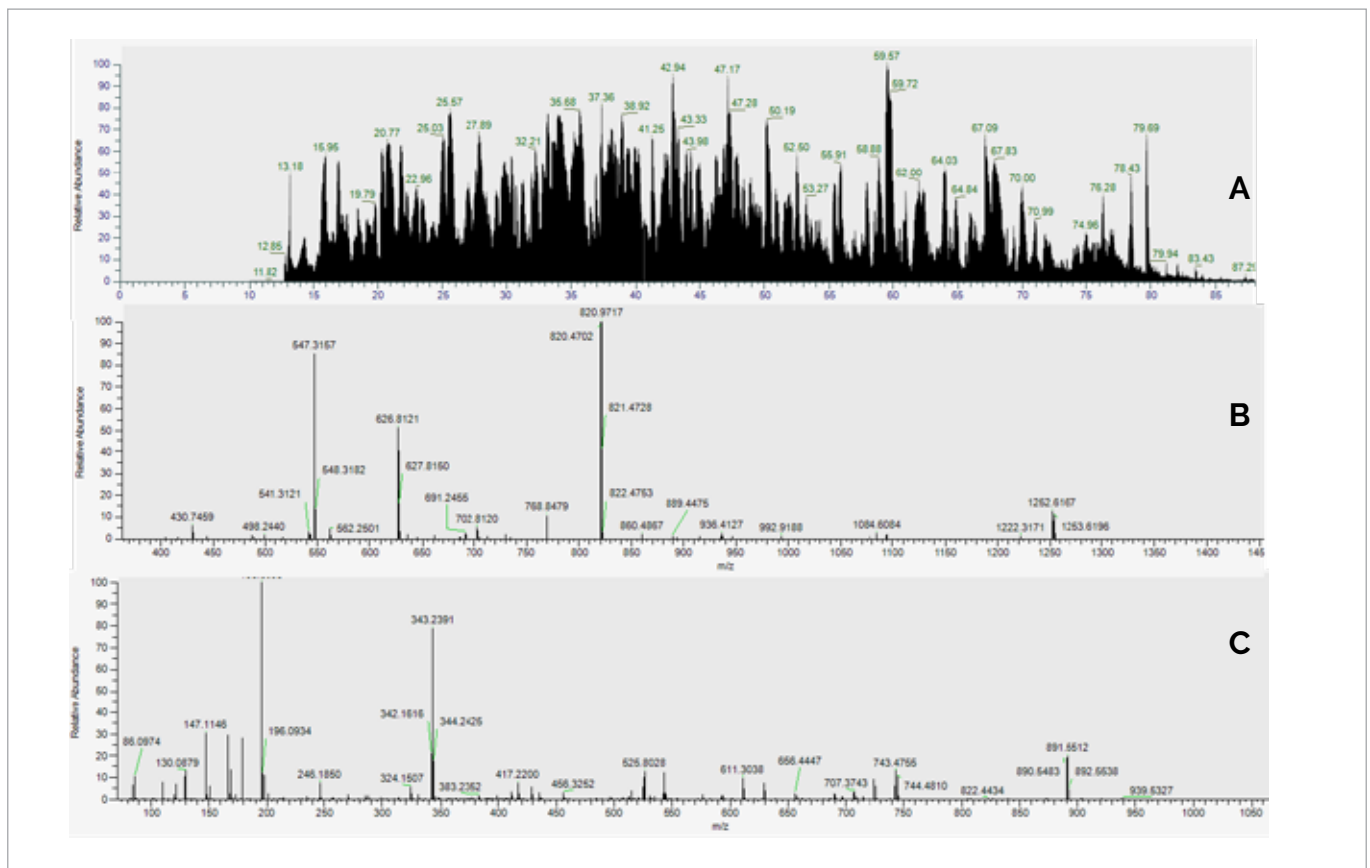
Figure 20: *A: Total ion chromatogram of a digested COVID-19 plasma sample; B: Parent ion spectrum from which ions were selected for fragmentation; C: MS/MS fragmentation spectrum used to identify the proteins in the sample.*
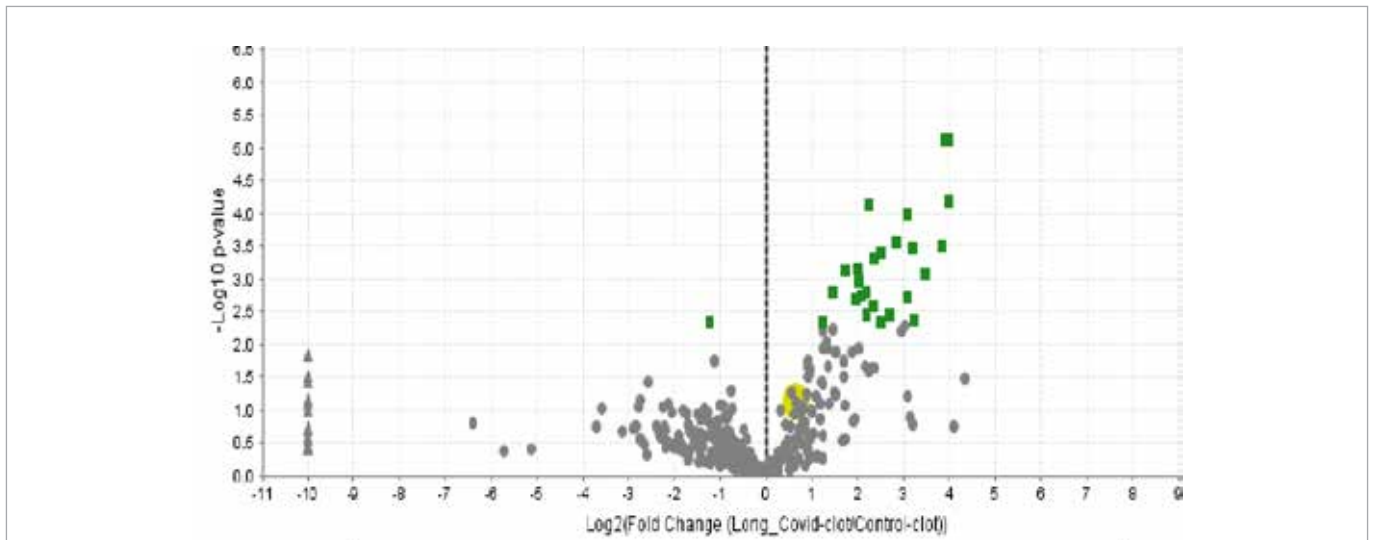
Figure 21: *Volcano plot depicting protein expression changes in long COVID patients relative to healthy controls.*

The digested material was subjected to nanoflow liquid chromatography-mass spectrometry/mass spectrometry on a Thermo Scientific high-resolution mass spectrometer. The proteomes were separated using a 90-minute gradient on a charged surface hybrid (CSH) column (Figure 20 A) before high-resolution spectra were acquired for protein identification (Figure 20 B and C) and quantitation (Figure 20 B and C). This was done by matching the experimental spectra obtained (Figure 20 C) to theoretical spectra using a combination of software. The software used was Thermo Scientific Proteome Discoverer and Scaffold Q+ from Proteome Software. The theoretical sequences were obtained from a previously published human-COVID-19 database.

The study found that in addition to the expected proteins such as fibrinogen, many anticoagulation-associated proteins and inflammatory markers were also trapped. The change in protein expression can be visualised using a volcano plot, as presented in Figure 21. The fold change is depicted on the x-axis in Log2 scale and the confidence (p-value) on the y-axis in -Log10 scale. The increase in alpha-2-antiplasmin may explain why long COVID-associated clots are not broken down as this protein is one of the central components in the fibrinolytic pathway. In addition to this, the discovery of 'trapped' inflammatory markers may also explain why symptomatic individuals receive serological tests within normal parameters – the markers tested for are trapped in the clots. Furthermore, a comparison between acute COVID-19 patients and long COVID patients showed a change in protein expression as the condition progressed from COVID-19 to long COVID. There was a marked increase in fibrinogen chains, serum amyloid A1 and 4 as well as von Willebrand factor, pointing to increased platelet activation.

The complete article with supporting information can be found in Cardiovascular Diabetology (*https://cardiab.biomedcentral.com/articles/10.1186/s12933-021-01359-7*). This work led to a follow-up study.

Insights achieved with volumetric electron microscopy

by Dr Jurgen Kriel

Electron microscopy (EM) has long been an essential tool for researchers to assess the ultrastructural detail of cells and tissues at nanoscale resolution. Although impactful, conventional EM approaches only relay information in a two-dimensional space, which limits the ability to assess the true structural organisation of biological material. From the way that connections amongst individual neurons are formed to how bacteria infiltrate plant roots, certain insights can only be gained once material is assessed in a three-dimensional space. Serial block-face (SBF) scanning electron microscopy (SEM) is a powerful volumetric EM modality that allows for such three-dimensional acquisition of information and was made available to researchers in Africa for the very first time at the end of 2020 by CAF.

The ThermoFisher Apreo Volumescope is one of the most recent and advanced volumetric SEMs available today. Housed at the Tygerberg Medical Campus, the Apreo Volumescope is the only such microscope on the African continent and opens the door to many new avenues of research in addition to the enhancement of current ongoing research.

Here, we provide the progress made in volumetric EM within the South African research landscape to showcase the novel insights that can be achieved through SBF-SEM.

In stark contrast to the brain tissue for which SBF-SEM was originally designed, the first South African study to make use of the Apreo Volumescope focused on characterising melanin-containing cells in lizard skin in order to understand how they are capable of changing colour under different weather conditions. The question posed by Dr Fredericco Masetti and Prof Susana Clusella-Trullas was whether the pigment-containing structures, referred to as melanophores, were shared amongst individual skin cells or whether these protrusions remained contained within the boundaries of single cells. The volumetric data revealed that the black pigmented structures (Figure 22) remained contained within the boundaries of distinct areas within the tissue sample, with melanophores protruding 'in between' other cells rather than being shared amongst them (displayed as purple rendered structures in Figure 22).
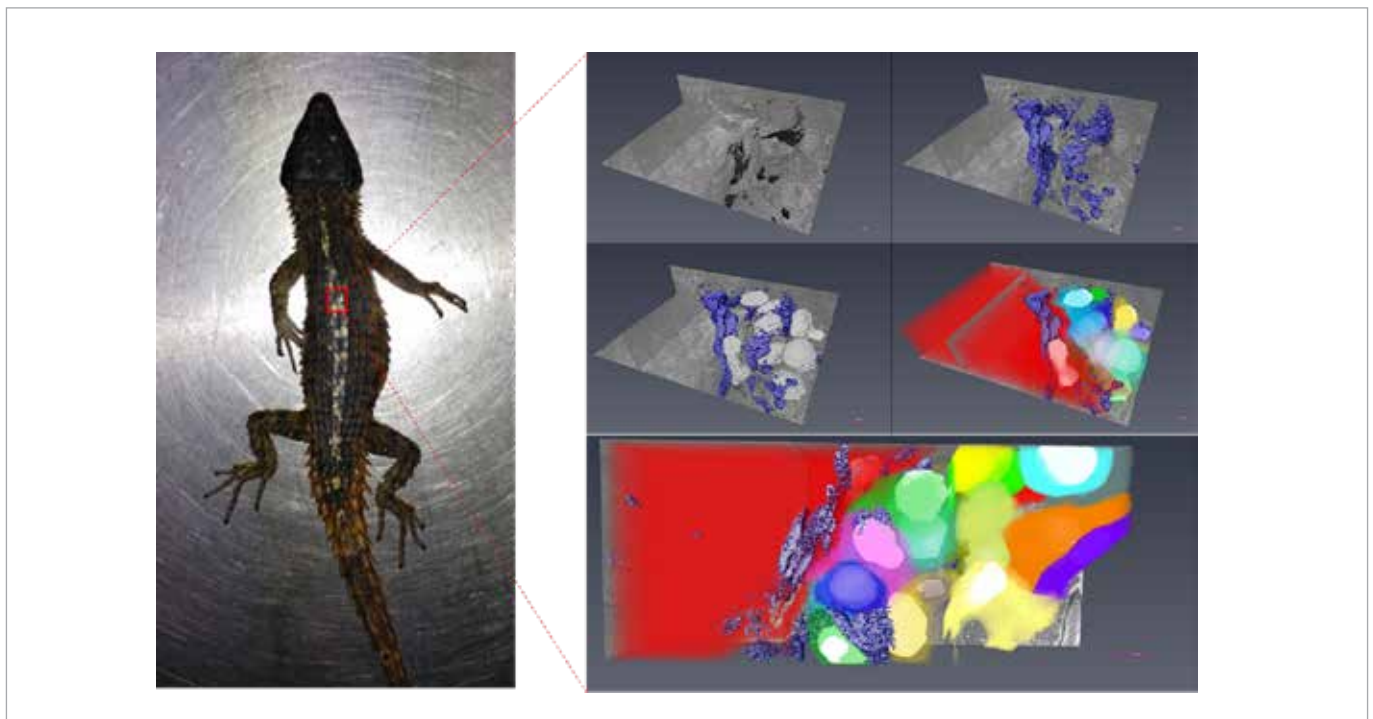
Figure 22: *Characterisation of melanophores in lizard skin. Scale bar 6 µm.*

Moving even further across disciplines, the Volumescope has also been utilised to understand pathogen interaction with plant material. As part of PhD candidate Alno Carstens' research (under supervision of Prof Lydia Joubert and Prof Gideon Wolfaardt), initial SEM analysis revealed bacterial association on the outer membrane of certain plant roots (Figure 23 A). However, it is not known whether these bacteria are able to penetrate the plant cell wall and if so, to what extent. SBF-SEM allowed for the visualisation of both plant material and bacterial association. Of note is that a single cross-section through the sample (Figure 23 B) would not accurately relay the extent of bacterial association. However, after subsequent image analysis and size exclusion-based thresholding (Figure 23 C, D), the spread of bacterial association was made visible, with only a small number of bacteria able to enter the plant.

Although the main aim of SBF-SEM is to render out structures of interest, it can also be used as an explorative tool. Three-dimensional cell culture models are greatly beneficial to cancer researchers as they mimic tumour growth in the human micro-environment more closely than single cells in a petri dish. However, a limiting factor in the ultrastructural analysis of cancer spheroids is being able to identify regions at different depths and to make accurate comparisons between the outer proliferating layer and the inner necrotic compartment. As part of MSc student Kim Frederick's thesis (under supervision of Prof Ben Loos), regional comparisons in the cytosolic ultrastructure could be made in brain cancer spheroids (Figure 24 A) at both the inner (Figure 24 B) and outer (Figure 24 C) layer in consecutive sections. This allowed for the identification and comparison in the volume of necrotic/dead regions between
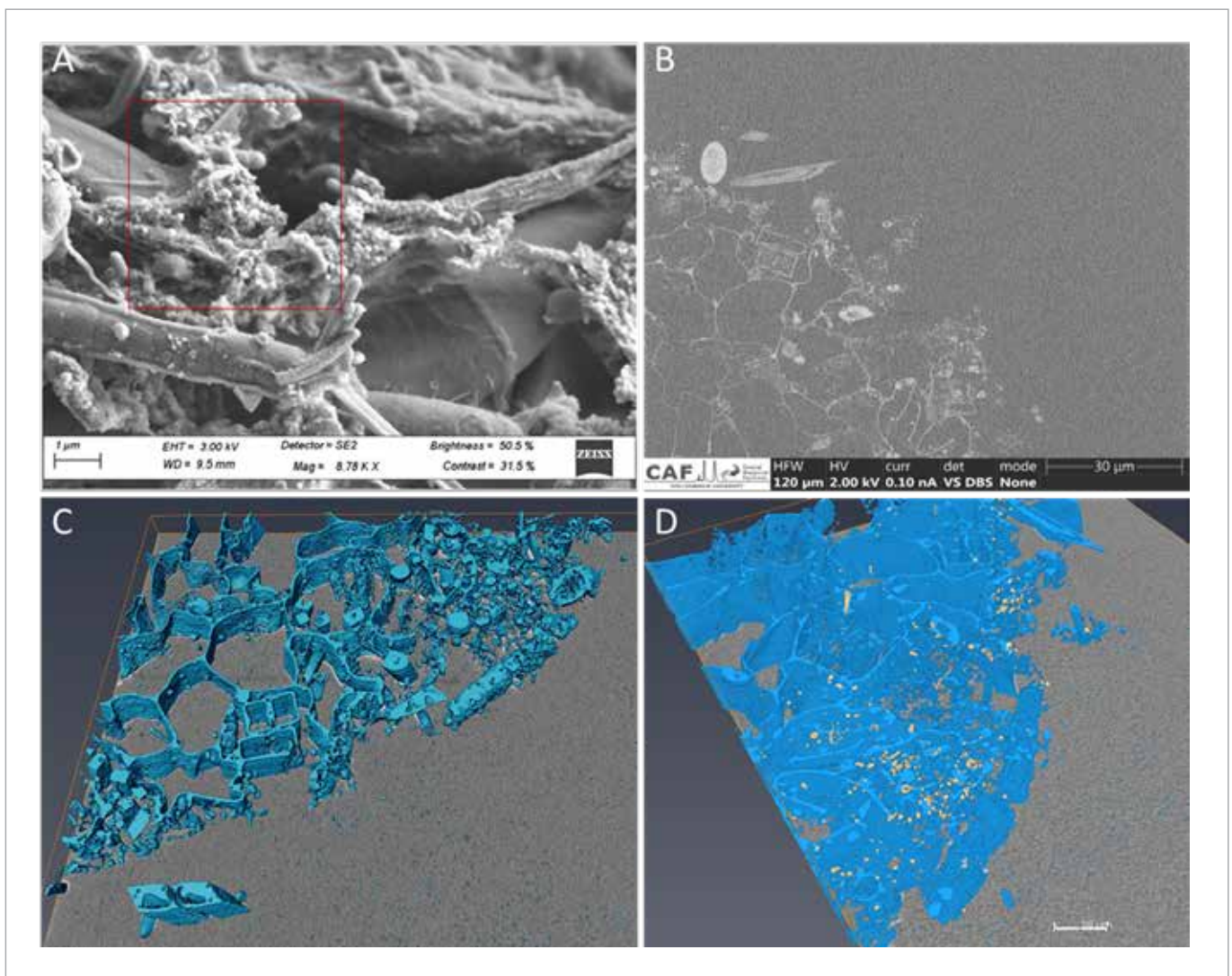
Figure 23: *Assessing bacterial interaction with Cyperus plant root. A) SEM image of dehydrated plant material. B) Single 50 nm section post resin embedding and staining. C) Volumetric render of all structures. D) Render of plant and bacterial structures.*
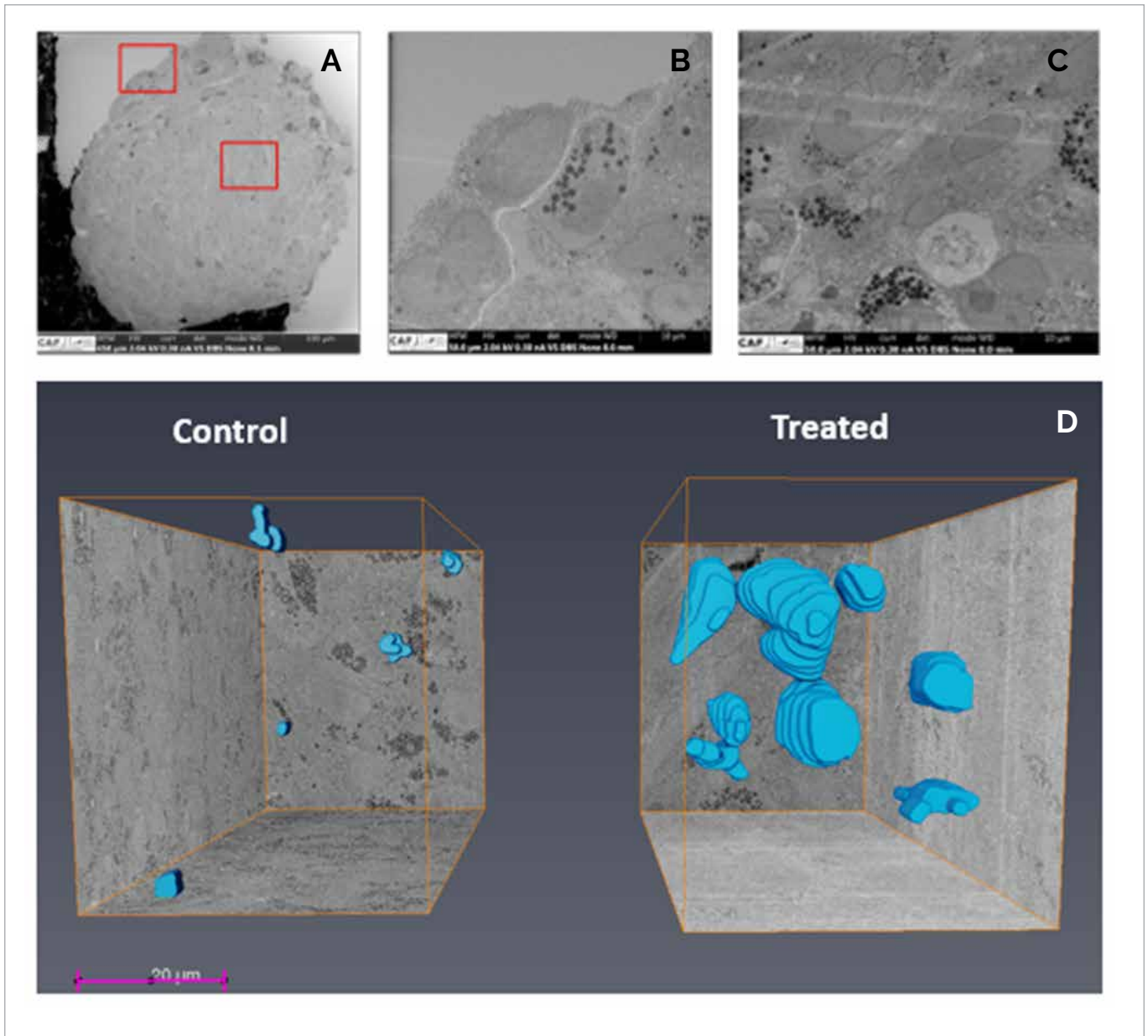
Figure 24: *Characterisation of necrotic regions in glioma spheroids. A) Overview of entire sample. B) Outer proliferating layer. C) Inner layer. D) Volumetric render and comparison of nectrotic areas.*
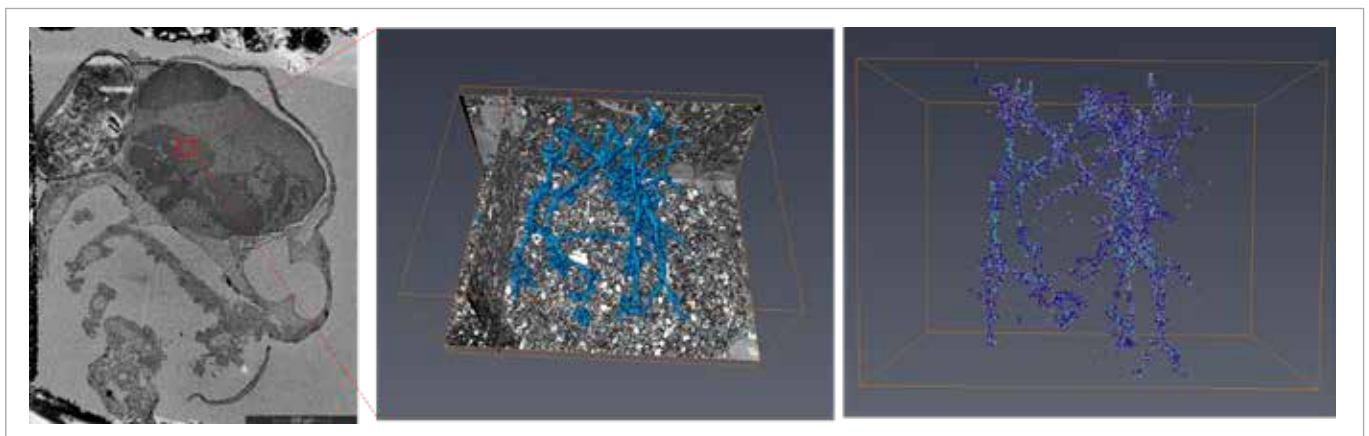
Figure 25: *Neuronal mapping in zebrafish. A) Overview of entire sample. B) Reconstruction of connected neurons. C) Network quantification of branching and terminal nodes.*

control and treated samples (Figure 24 D) to study the potential therapeutic outcomes of novel compounds.

Connectomics is the field of study dedicated to mapping neuronal circuitry in order to identify specific pathways associated with behaviour or to establish how neuronal interactions become damaged under pathological conditions. Although an area of great advancement in the rest of the world, such research has never before been possible in South Africa. Since the acquisition of the Apreo Volumescope, Dr Kriel has worked closely with Prof Carine Smith to make connectomics research possible in South Africa. Using zebrafish as a model organism, they have been able to segment connected neurons in a subset of zebrafish brain tissue. Currently, efforts are being made to conduct this segmentation automatically using deep learning-based approaches. Figure 25 shows the mapping of a connected subset of neurons and quantification of the network connections in a single circuit.

The Central Analytical Facilities (CAF) Microscopy Unit remains the only microscopy unit in South Africa dedicated to the advancement of multimodal imaging. Although 2D correlative light and electron microscopy (CLEM) is now a streamlined service, 3D CLEM has long been out of reach for South African researchers. CAF has now successfully set up a 3D CLEM workflow to combine confocal and volumetric EM datasets. This approach is currently aiding infectious disease researchers Dr Caroline Beltran and Prof Gerhard Walzl to enhance the understanding of *Mycobacterium tuberculosis* (mTB) pathophysiology, specifically in the formation of granulomas. Comprised of a variety of immune cells, assessing the distribution of mTB-infected cells in granulomas is made possible by genetic modification of mTB to produce a fluorescent protein. Image B in Figure 26 shows a confocal microscopy image render of granuloma in mouse lung tissue, with the mTB in the red fluorescence channel. Although this allows for the combined visualisation of multiple immune cell markers, the individual bacteria within each infected cell

cannot be adequately studied through light microscopy alone. Through a series of careful sample preparation steps, SBF-SEM was conducted on a single granuloma after it had been identified through confocal microscopy (Figure 26 A – E). Overlaying these two datasets gave a clear indication of where the bacteria were located (Figure 26 E – G) and allowed for the segmentation of individual bacteria within infected macrophages. Furthermore, the multinucleated nature of these cells could also be more accurately studied, and preliminary data suggest that these infected cells form an organised network (Figure 26 G).

Figure 26 A) Confocal tile scan of mouse lung vibratome section. B) Render of confocal image stack (60 x magnification). C) Flat resin embedding and fine cutting of region of interest (ROI). D) SBF-SEM overview image of entire ROI during acquisition. E) Overlay of confocal and SBF-SEM images, with high-resolution ROI outlined in red. F) Region positively identified to contain bacteria. G) Render of infected cells. H) Combined surface render of a single macrophage (green) contained multiple nuclei (grey) and mTB (red).

The data presented here is a remarkable display of how researchers from various disciplines can gain valuable insights through volumetric EM. Though much progress has been made, the application of SBF-SEM is still in its infancy in South Africa. It is hoped that with further expansion of the skills and expertise necessary to acquire and process SBF-SEM datasets, novel discoveries can be made to pave the way for advances in critical sectors ranging from healthcare to agriculture.

Reference list

1. Ramón y Cajal, S. *Histologie du système nerveux de l'homme & des vertébrés.* Vol. 1 (Maloine, 1909).
2. Denk, W. & Horstmann, H. Serial Block-Face Scanning Electron Microscopy to Reconstruct Three-Dimensional Tissue Nanostructure. PLOS Biol. 2, e329 (2004).
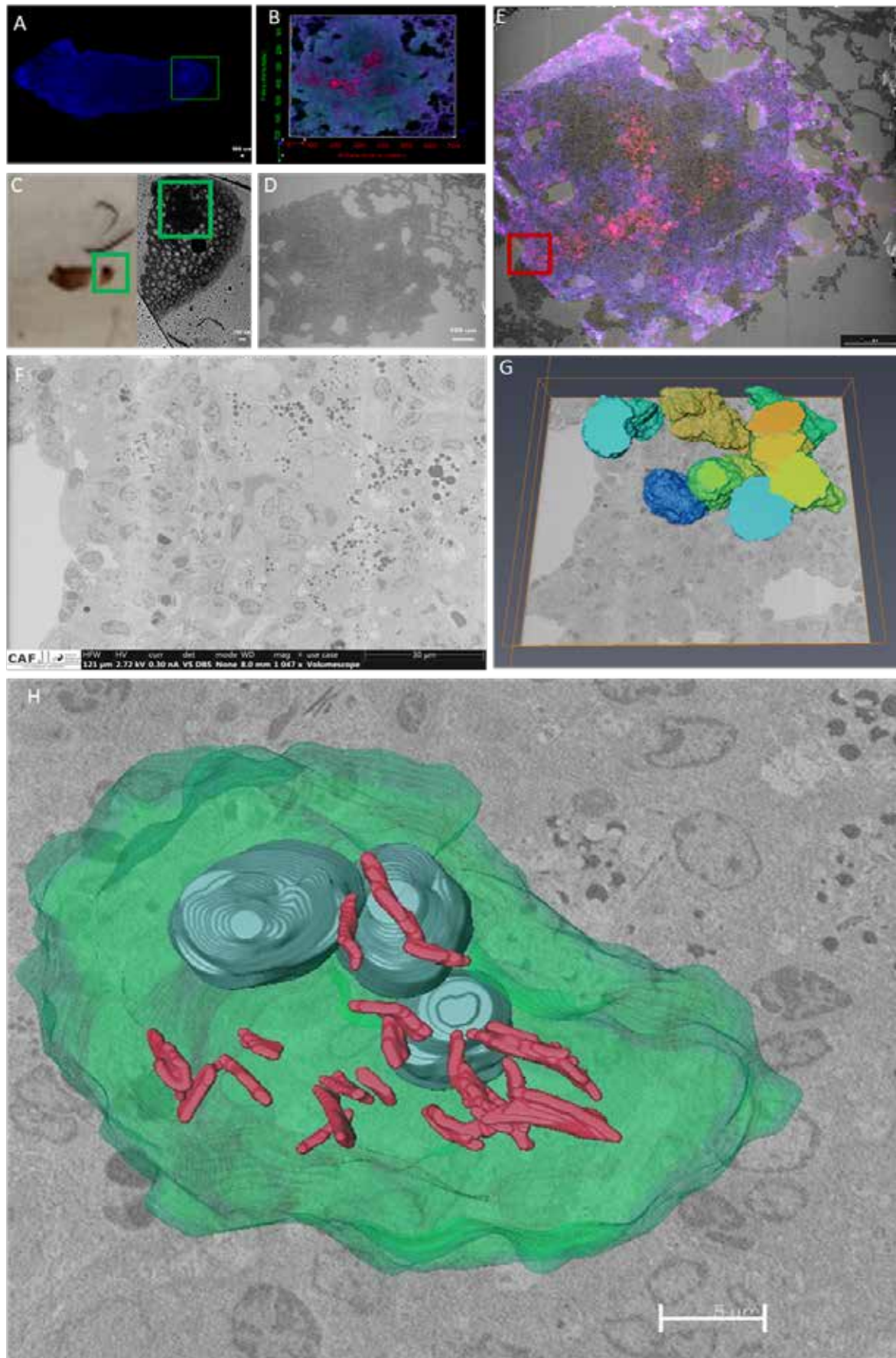
Figure 26: *A) Confocal tile scan of mouse lung vibratome section. B) Render of confocal image stack (60 x magnification). C) Flat resin embedding and fine cutting of region of interest (ROI). D) SBF-SEM overview image of entire ROI during acquisition. E) Overlay of confocal and SBF-SEM images, with high-resolution ROI outlined in red. F) Region positively identified to contain bacteria. G) Render of infected cells. H) Combined surface render of a single macrophage (green) contained multiple nuclei (grey) and mTB (red).*

Imaging and full-spectrum flow cytometers at CAF first in South Africa

Figure 27: *Diatom blooming events (brown-tinted patches in the water) captured at Muizenberg beach.*

By Dr Dalene de Swardt

The Flow Cytometry Unit, of which most of the instruments are based at the Tygerberg campus, proudly houses state-of-the-art flow cytometers of which two of the instruments were the first to be installed in South Africa. The Luminex AMNIS® ImageStreamX Mk II (installed in 2019) was the first imaging flow cytometer in Africa, and the Cytek® Aurora flow cytometer (installed in 2021) was the first full-spectrum instrument to arrive in South Africa (the first African country to obtain the instrument was Uganda). The addition of these instruments to the Central Analytical Facilities' (CAF) Flow Cytometry 'playground' immensely broadened the scope of what the Flow Cytometry Unit could offer to academia and interested groups from the private sector. Furthermore, these instruments have been very useful when conventional flow cytometry needed a microscopic insight (AMNIS ImageStream flow

cytometer) and when the exclusion of impeding autofluorescence and a greater-than-13 para-meter platform were required to better under-stand, specifically, cellular morphology and function (Cytek Aurora full-spectrum flow cytometer). Here, we would like to highlight some of the research fields that explored the new technology and the fascinating analyses observed since the instruments have entered the Flow Cytometry Unit.

Visitors to the Flow Cytometry Unit included the Marine Ecology Research Group from the University of Cape Town. The researchers, Prof Colleen Moloney, Dr Emma Rocke and MSc student, Casha de Vos, were interested to see whether the AMNIS ImageStream could assist with detecting phyto-plankton, known as diatoms (*Anaulus australis*), from coastal water samples. The researchers also wanted to utilise the instrument's ability to provide a more

rapid statistical output compared to the use of a microscope, with which defining and counting diatoms are an extremely time-consuming activity. Samples were taken from Muizenberg Beach, False Bay, at the time of diatom blooming, a term that describes the diatoms in the phase of rapid asexual reproduction that becomes evident as patches of coastal water takes on a brownish tint, often mistaken as water pollution (Figure 27). The research group processed the sample for acquisition using the AMNIS ImageStream, which caused much excitement when the first images of the diatoms came into view.
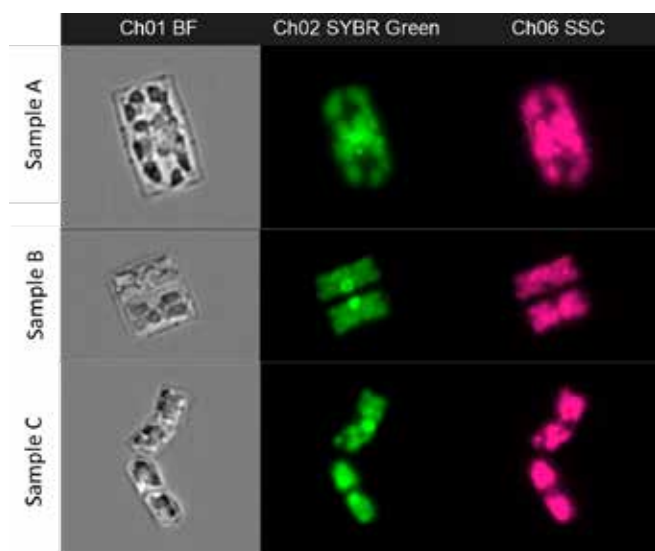
Figure 28: *AMNIS ImageStream images of diatoms showing brightfield (Ch01 BF), green fluorescent images from the SYBR green DNA stain dye (Ch02 SYBR green) and internal complexity (Ch06 SSC)*

The diatoms were stained with a fluorescent dye (SYBR green) that binds to double-stranded DNA. Fluorescent light is excited by the 488 nm (blue) laser and emitted light were detected as a green signal on the visible spectrum. The images in Figure 28 show the brightfield image (Ch01 BF) of the diatoms as would have been observed with conventional light microscopy. The images of the Ch02 SYBR green column are from the DNA-stained diatoms, and the pink colour images are from the Ch06 SSC (side scatter) column that defines the degree of internal complexity. The latter profile is obtained when the blue laser is also employed to collect information from, specifically, the 90-degree light deflection pattern generated from each cell. Sample A shows a single rectangle-shaped diatom, and samples B and C depict two rectangle- shaped diatoms differently positioned to each other.

To date, the AMNIS ImageStream has played a significant role in studies that focused on various biological (*Mycobacterium smegmatis, Mycobacterium bovis*, murine macrophages, human lymphocytes, yeast, algae, pollen, mature biofilms, etc.) and synthetic (various types of nanoparticles) entities as well as in various applications (converting a microscopy-based fluorescent in situ hybridisation [FISH] technique to flow cytometry, infection, toxicity, apoptosis, phagocytosis, etc.). This year, the AMNIS ImageStream will also contribute to a study investigating extracellular vesicles, a new and evolving research niche.

A concept in flow cytometry that majorly complicates analyses is autofluorescence. This is defined as light that is emitted from the inherent molecules of cells, which act as natural fluorescent probes and hinder the detection of exogenous fluorescent probes employed to assist in studying specific morphological and functional characteristics of cells. This is especially problematic in a clinical setting. As an example, macrophages from bronchoalveolar lavage (BAL) are cells notorious for eliciting a high autofluorescent signal. These samples are currently being investigated as part of a Tuberculosis (TB) study by the Immunology Research Group of the Department of Molecular Biology and Human Genetics, Faculty of Health Sciences, Stellenbosch University. Preliminary data obtained in using the Cytek Aurora full-spectrum flow cytometer, demonstrated the instrument's role as an indispensable tool for conducting the study as it was able to extract the impeding autofluorescent signal, which greatly assisted with accurate analyses of sample data. Figure 29 illustrates the data that was collected using conventional flow cytometry versus full-spectrum flow cytometry by the study group.

In addition to correcting for autofluorescence, the Cytek Aurora full-spectrum flow cytometer has expanded the Flow Cytometry Unit's capability to now allow for the analysis of up to 48 parameters simultaneously (the conventional flow cytometer at the Flow Cytometer Unit can only analyse 13 parameters, simultaneously). Notably, as the number of parameters of interest increases, the complexity regarding the design to include a high number of parameters in one assay or panel also intensifies. A range of factors needs to be taken into account during the design for an accurate data output. Nevertheless, the output is very rewarding as it immensely

expands data collection and our knowledge of the particular cells of interest. Currently, Ms Andrea Gutschmidt, Technical Officer with the TB study group, with guidance of the full-spectrum flow cytometer specialist, Ms Maria Jaimes from Cytek Biosciences, is designing a 30-parameter flow cytometry panel. Once this process is completed, it will be the first 30-parameter flow cytometer panel to be acquired and analysed at the Flow Cytometry Unit. This is a great achievement towards the growth of the technology and expertise development at Stellenbosch University.
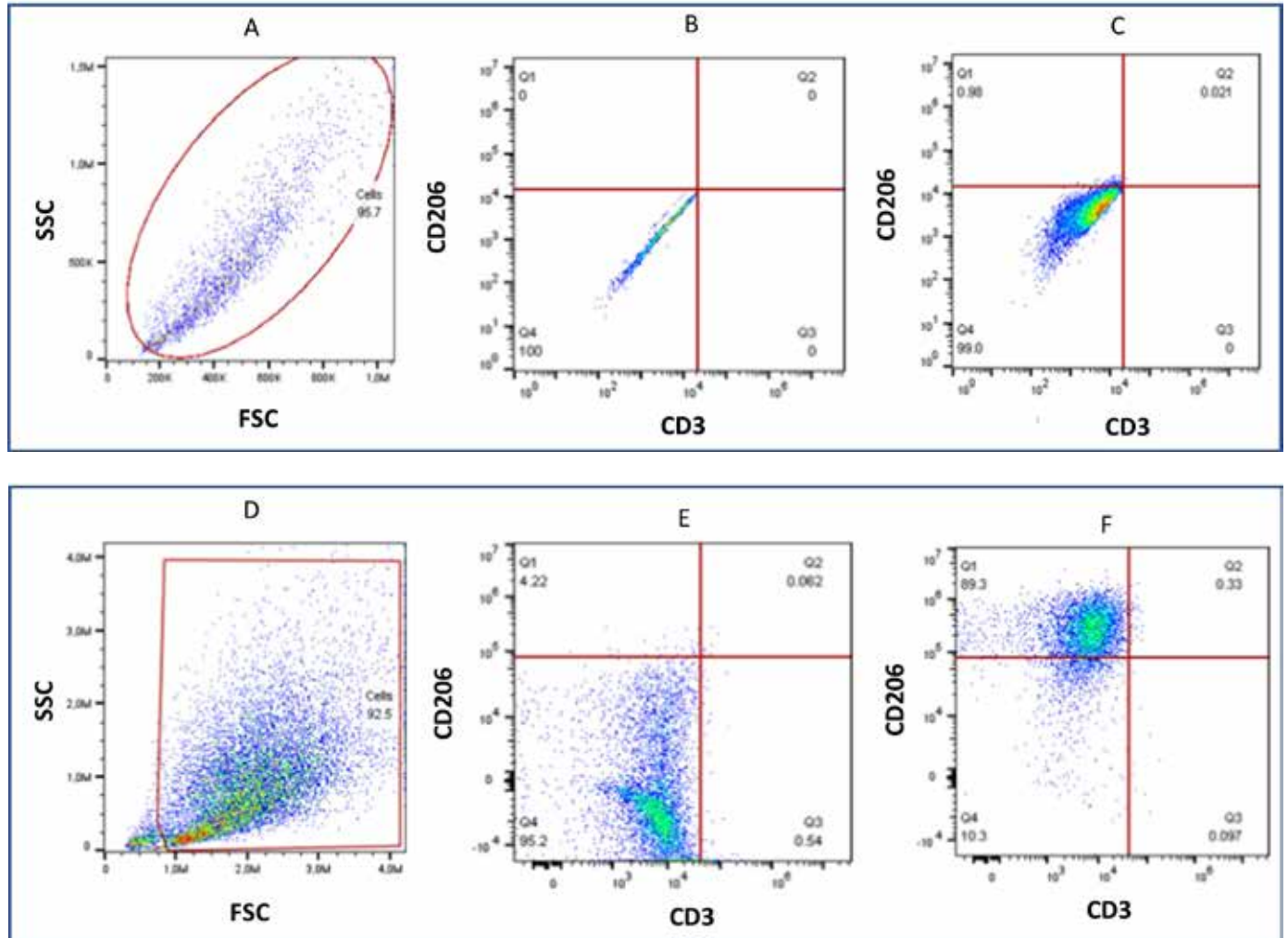
Figure 29: *Autofluorescence in conventional versus full-spectrum flow cytometry. Graphs A, B and C show data on BAL samples that were collected using a conventional flow cytometer compared to graphs D, E and F that show data from a similar sample collected using the full-spectrum flow cytometer. Graphs A and D show cells from BAL fluid identified according to their size (FSC) and granularity (SSC) and collected as indicated by the red enclosed gates. These cells were further investigated for their cell surface expression by staining with exogenous fluorochromes that would identify the CD3 and CD206 cell surface markers. Graphs B and E show the profile of the unstained BAL sample that is used to guide analysts in defining the boundaries of the negative exogenously stained fluorescent events. Graph B shows the signature profile of autofluorescence with conventional flow cytometry, whilst Graph E depicts the extracted autofluorescent signal performed by full-spectrum flow cytometry. In comparing Graph C to Graph B, a change in the profile of the cell population is observed but is difficult to measure due to the impeding autofluorescent signal, whilst in Graph F, post the extraction of the fluorescent signal, the positive fluorescence from the exogenous signal is clearly detectable and true marker-positive events can be analysed.*

Financial Reports

By Fransien Kamper

		January 2018-31 December 2018	January 2019-31 December 2019	Total on 31 Dec 2020	Total on 31 Dec 2021	Budget 2022
MS Unit	Internal invoicing	2 040 163	1 893 475	1 033 947	1 599 311	1 211 347
	External invoicing	5 148 560	6 803 566	5 661 872	7 971 178	9 771 783
	Total logbook income	**7 188 723**	**8 697 041**	**6 695 819**	**9 570 489**	**10 983 130**
	Expenses			0		
	Salaries	3 708 383	4 202 003	4 645 421	4 521 704	4 537 373
	ICR	875 255	1 360 713	1 132 374	1 618 314	1 724 584
	Running costs	906 574	1 171 430	849 691	1 083 715	1 258 260
	Maintenance	829 955	905 603	962 537	375 552	1 323 530
	Travel costs	11 805	281			
	Small equipment & KKW	70 461	5 952	21 860	71 415	
	Deferred costs		255 800		399 996	439 993
	Total expenses	**6 402 433**	**7 901 782**	**7 611 884**	**8 070 697**	**9 283 739**
FM Unit	Internal invoicing	1 261 988	856 494	573 022	1 407 422	516 958
FROM 2022 Flow Cytometry Unit	External invoicing	74 017	189 215	109 064	78 438	17 716
	Total logbook income	**1 336 005**	**1 045 709**	**682 086**	**1 485 860**	**534 674**
	Expenses					
	Salaries	889 764	930 059	1 023 435	1 064 557	761 011
	ICR	12 583	37 843	21 813	15 688	3 231
	Running costs	313 664	425 804	92 688	118 138	92 919
	Maintenance	79 978	59 150	108 802	589 302	282 984
	Travel costs	3 674	6 653	334		
	Small equipment & KKW	36 455	114 407			
	Deferred costs		150 000		150 000	165 000
	Total expenses	**1 336 118**	**1 723 916**	**1 247 071**	**1 937 684**	**1 305 146**
SEM Unit	Internal invoicing	948 918	918 242	687 982	1 184 639	1 721 395
FROM 2022 Microscopy Unit	External invoicing	2 107 221	732 351	757 935	1 097 588	1 138 866
	Total logbook income	**3 056 139**	**1 650 593**	**1 445 917**	**2 282 227**	**2 860 261**
	Expenses					
	Salaries	2 100 941	1 684 505	1 389 647	1 566 323	2 384 880
	ICR	358 228	146 470	151 587	219 451	207 729
	Running costs	196 673	62 968	98 324	112 013	345 758
	Maintenance	35 975	93 673	23 065	93 509	244 109
	Travel costs	64 975	5 491	3 473		23 592
	Small equipment & KKW	177 800	86 628	3 635	75 347	
	Deferred costs		120 000		120 000	132 000
	Total expenses	**2 934 592**	**2 199 735**	**1 669 731**	**2 186 643**	**3 338 068**

		January 2018-31 December 2018	January 2019-31 December 2019	Total on 31 Dec 2020	Total on 31 Dec 2021	Budget 2022
ICP & XRF Unit	Internal invoicing	1 045 643	1 005 564	549 250	881 442	915 595
	External invoicing	2 759 674	2 366 846	1 957 142	3 470 563	4 111 588
	Total logbook income	3 805 317	3 372 410	2 506 392	4 352 005	5 027 182
	Expenses					
	Salaries	2 417 316	2 709 331	2 026 864	2 191 359	2 291 562
	ICR	469 145	473 369	391 428	695 463	749 954
	Running costs	857 977	1 005 950	708 254	650 152	987 300
	Maintenance	539 500	1 156 984	400 981	343 292	721 026
	Travel costs	77 034	62 089	9 182	60 768	56 367
	Small equipment & KKW	29 597	66 476		41 604	4 099
	Deferred costs		354 613		399 997	439 993
	Total expenses	4 390 569	5 828 812	3 536 709	4 382 635	5 250 299
DNA Unit	Internal invoicing	4 690 289	3 774 647	2 925 162	4 199 985	3 595 684
	External invoicing	6 259 800	5 752 054	4 158 801	5 499 622	5 764 144
	Total logbook income	10 950 090	9 526 701	7 083 963	9 699 607	9 359 828
	Expenses					
	Salaries	2 986 764	3 089 240	3 400 922	4 169 205	3 507 405
	ICR	1 064 166	1 150 411	831 760	1 099 924	1 051 380
	Running costs	6 669 796	5 604 611	5 531 489	5 217 755	4 555 541
	Maintenance	255 726	175 405	143 324	131 906	17 866
	Travel costs	774	831			
	Small equipment & KKW		51 228	83 118	52 995	105 743
	Deferred costs		133 333		285 000	313 500
	Total expenses	10 977 226	10 205 059	9 990 613	10 956 786	9 551 436
NMR Unit	Internal invoicing	697 665	660 625	565 437	467 698	700 332
	External invoicing	641 179	910 628	421 555	307 035	732 686
	Total logbook income	1 338 844	1 571 254	986 992	774 734	1 433 018
	Expenses					
	Salaries	1 342 756	1 429 138	1 217 297	1 805 929	1 615 643
	ICR	109 000	182 126	84 311	61 407	70 338
	Running costs	383 393	517 358	563 174	465 393	328 486
	Maintenance	12 678	48 897	-1 236	75 053	10 494
	Travel costs		2 911	12		
	Small equipment & KKW			10 427		
	Deferred costs					
	Total expenses	1 847 827	2 180 430	1 873 985	2 407 782	2 024 962

		January 2018- 31 December 2018	January 2019- 31 December 2019	Total on 31 Dec 2020	Total on 31 Dec 2021	Budget 2022
CT Scanner Unit	Internal invoicing	663 253	490 600	321 330	287 051	721 113
	External invoicing	2 764 088	1 551 760	1 303 930	1 657 187	1 104 741
	Total logbook income	3 427 341	2 042 360	1 625 260	1 944 237	1 825 854
	Expenses					
	Salaries	1 563 400	1 646 964	1 259 025	1 396 339	615 486
	ICR	469 895	310 352	260 786	263 351	277 856
	Running costs	408 092	277 121	309 351	149 628	235 046
	Maintenance	313 044	565 225	156 774	492 889	70 470
	Travel costs	24 491	58 676	327		
	Small equipment & KKW	42 057		25 243	60 912	
	Deferred costs		341 108		350 003	385 007
	Total expenses	2 820 979	3 199 446	2 011 507	2 713 122	1 583 865
Neurome- chanics Unit	Internal invoicing	569 253	323 158	203 044	271 713	164 400
	External invoicing	826 252	1 069 544	954 667	1 123 225	829 198
	Total logbook income	1 395 504	1 392 703	1 157 711	1 394 938	993 598
	Expenses					
	Salaries	1 475 937	2 060 312	2 107 151	1 382 867	794 396
	ICR	140 463	213 909	190 933	224 645	165 840
	Running costs	46 213	70 248	22 299	49 810	25 396
	Maintenance	66 010	43 315	23 802	18 501	4 550
	Travel costs	15 589	72 581			
	Small equipment & KKW	55 196	48 070	49 449		
	Deferred costs		68 711		99 997	99 996
	Total expenses	1 799 407	2 577 146	2 393 635	1 775 819	1 090 178
Vibrational Spectroscopy Unit	Internal invoicing	57 175	104 529	57 450	102 940	143 974
	External invoicing	18 264	44 949	5 250	4 416	2 750
	Total logbook income	75 439	149 478	62 700	107 356	146 724
	Expenses					
	Salaries	407 321	595 708			
	ICR	3 105	8 990	1 050	883	502
	Running costs	7 636	7 824	3 857	2 773	2 047
	Maintenance					
	Travel costs					
	Small equipment & KKW					
	Deferred costs		25 008			109 993
	Total expenses	418 062	637 530	4 907	3 656	112 542

		January 2018-31 December 2018	January 2019-31 December 2019	Total on 31 Dec 2020	Total on 31 Dec 2021	Budget 2022
TOTAL UNITS INCOME	Total internal income	11 974 346	10 027 336	6 916 624	10 402 199	9 690 797
	Total external income	20 599 056	19 420 912	15 330 215	21 209 252	23 473 471
	Total income: all units	32 573 402	29 448 248	22 246 839	31 611 451	33 164 268
ADDITIONAL INCOME						
	Interest received	465 843	1 511 454	353 657	849 006	782 730
	Funds received VR(R)	750 000	750 000	750 000		1 000 000
	Salary contribution VR(R)	3 952 335	4 203 342	4 355 720	4 346 081	5 212 899
	Infrastructure NII repayment		2 000 000			
	US loan / ALT 2020 funds: detector CT		2 321 000			
	VAT refund on equipment		94 451			
	Faculty contributions					
	NII levy			142 324	180 000	180 000
	BIOGRIP levy				44 156	40 000
	VAT refund on equipment				5 357 647	1 255 455
	TOTAL ADDITIONAL INCOME	5 168 178	10 880 247	5 601 701	10 776 890	8 471 084
TOTAL INCOME		37 741 580	40 328 495	27 848 540	42 388 341	41 635 351
EXPENDITURE	TOTAL EXPENDITURE					
	Expenses					
	Salaries					
	Salaries: admin	1 983 822	2 184 381	2 355 196	2 482 196	2 529 520
	Salaries: units	16 892 583	18 347 259	17 069 762	18 098 282	16 507 756
	Salaries: bonus	299 326				
	17% / 20% ICRR (Indirect Cost Recovery)	3 501 839	3 884 182	3 066 043	4 199 126	4 251 413
	Running costs (sum of units)	9 790 017	9 143 314	8 179 127	7 849 376	7 830 753
	Maintenance (sum of units)	2 132 866	3 048 251	1 818 049	2 120 005	2 675 029
	Travel costs (sum of units)	198 342	209 513	13 328	60 768	79 959
	Small equipment & KKW (sum of units)	411 566	372 761	193 732	302 273	109 842
	Deffered costs		1 448 573		1 804 993	2 085 481
	CAF general running costs	674 184	592 964	468 200	411 876	424 795
	Students		342 663	350 338	201 596	170 000
	Interest			17 224	21 382	
	Travel costs-courier	80 034	89 313	69 883	69 688	68 000
	Development new labs		1 121 212			
	Infrastructure	29 989	115 217	11 804	589 394	89 995
	Infrastructure NII					
	Equipment	608 733	27 648	77 071	17 135	31 924
	NMR purchase				698 031	
	HPLC				1 000 000	
	Maintenance			23 336		
	Equipment repair: CT Scanner		2 344 334	519 207		
	Equipment repair fund	500 000			500 000	500 000
	CAF vehicle fund	45 000			45 000	45 000
	Equipment replacement fund				4 000 000	4 000 000
	Total normal operational costs	37 148 302	43 271 587	34 232 299	44 471 122	41 399 468

		January 2018-31 December 2018	January 2019-31 December 2019	Total on 31 Dec 2020	Total on 31 Dec 2021	Budget 2022
	Surplus per year before special income	593 278	-2 943 092	-6 383 759	-2 082 781	235 883
Special Additional Income	COVID insurance claim note 2			5 000 000		
Surplus/Shortfall	Surplus/Shortfall per year	593 278	-2 943 092	-1 383 759	-2 082 781	235 883
	CAF overdraft (Originally Rmilj Facility)			10 000 000		
EQUIPMENT EXPENDITURE			35 997 603		38 181 619	
	NRF-NEP total grants		23 982 455		7 120 740	
	ALT/US funds		8 000 000		3 560 370	
	Loan: 2020 ALT		2 643 935			
	Contributions: Faculty of Science		500 000			
	CAF contribution		871 213			
	ALT FUNDS - NMR purchase				12 402 478	
	Science Faculty: contribution NMR				10 000 000	
	Strategic Funds: NMR				4 400 000	
	CAF contribution: NMR				698 031	
NEP EQUIPMENT DETAILS			35 997 601		38 181 619	
	Mass-Directed Auto Purification & QC system		9 431 805			
	Amnis Image StreamX MarkII Imaging Flow Cytometer		12 673 106			
	Gemini 300FESEM with advanced system for automated 3D		13 892 690			
	Spectral Flow Cytometer				10 681 110	
	400MHZ and 600MHZ nuclear magnetic resonance				27 500 509	
FUNDS						
	Emergency equipment repair fund	1 582 635	1 688 915	1 078 605	1 618 027	2 118 027
	Vehicle Replacement	160 930	239 363	248 948	302 546	347 546
	Reserve, food security project	1 201 041	1 214 773	1 221 614	1 229 267	1 229 267
	Maintenance fund equipment: BD FACS Jazz sorter (2013)	1 185 280	1 214 029	1 240 769	1 394 496	1 394 496
	Provision for leave payments				769 262	901 298
	Equipment replacement				4 000 000	8 000 000
	Deffered costs		1 448 573	1 448 573	3 143 230	5 228 711
		4 129 885	5 805 653	5 238 509	12 456 829	19 219 345

		CAF UNITS: Financially ring-fenced DSI funded research infrastructure platform nodes				

		STELLENBOSCH UNIVERSITY: CENTRAL FACILITIES FINANCIAL REPORT: NII				
		2017-2018	January 2019- 31 December 2019	January 2020- 31 December 2020	January 2021- 31 December 2021	BUDGET 2022
NII	NODE funding	26 315 789	381 396	3 742 420	3 000 000	2 535 750
	Bridging funding	19 000 000	-6 831 086			
	VAT refund on equipment					3 084 593
	Interest received	2 720 338	1 566 713	282 219	199 879	190 000
	Income			869 559	1 211 787	1 606 890
	Private patients			939 909	4 112 235	4 559 375
	Total income	48 036 127	-4 882 977	5 834 107	8 523 900	11 976 608
	Expenses					
	Salaries & running costs	1 080	2 109 155	5 240 134	8 800 612	9 266 512
	Building & equipment		32 213 533	3 122 671	366 473	
	Equipment replacement fund					3 500 000
	Total expenses	1 080	34 322 688	8 362 806	9 167 085	12 766 512
	Year end balance	48 035 047	8 829 383	6 300 684	5 657 499	4 867 595

		STELLENBOSCH UNIVERSITY: CENTRAL FACILITIES FINANCIAL REPORT: BIOGRIP				
			1 April 2019- 31 March 2020 Year1	1 April 2020- 31 March 2021 Year 2	1 April 2021- 31 March 2022 Year 3	1 April 2022- 31 March 2023 Year 4
BIOGRIP	NODE funding		5 842 139	7 480 163	5 370 719	8 181 221
NODE funding	Interest received					
	Income					
	Total income		5 842 139	7 480 163	5 370 719	8 181 221
	Expenses					
	Salaries & running costs		827 288	2 755 802	2 809 405	4 504 892
	ICR (indirect cost recovery)		292 107	374 008	268 536	409 061
	Equipment		4 726 110	4 085 475	1 752 548	3 267 268
	Total expenses		5 845 505	7 215 284	4 830 489	8 181 221
	Balance for each grant period		-3 366	264 879	540 230	0
BIOGRIP-CAF activities	Income CAF activities			263 207	583 095	600 000
	Interest received		19 425	288 175	46 373	40 000
	Total income		19 425	551 382	629 468	640 000
	Expenses					
	Salaries & running costs			45 360		
	Deffered costs					500 000
	ICR (indirect cost recovery)			2 583	51 191	50 000
	Total expenses		0	47 943	51 191	550 000
	Surplus each period		19 425	503 438	578 277	90 000

NOTE 1: ICR costs have been shifted to reflect on the unit costs, to the revenue to which they relate.

NOTE 2: Covid Insurance claim paid.

NOTE 3: BIOGRIP NODE is reported in periods as to be reported to BIOGRIP HUB
Income for Year 3 - not yet received from the HUB

NOTE 4: In January 2022 the FM (Fluorescence Microscopy Unit, offering both microscopy and flow cytometry services) and SEM Units were restructure and split up into two new Units: Microscopy (Fluorescence Microscopy and Electron Microscopy) and Flow Cytometry.

Graphs detailing aspects of CAF income during 2021

Figure 30: *Percentage of income derived from the different categories of clients for 2021.*

SU Clients	32,51%
Industry Clients (RSA)	28,73%
Clients from other SA Universities	24,76%
International Client	7,44%
RSA Research Institution	5,51%
Non-South African University	1,02%
Private	0,03%
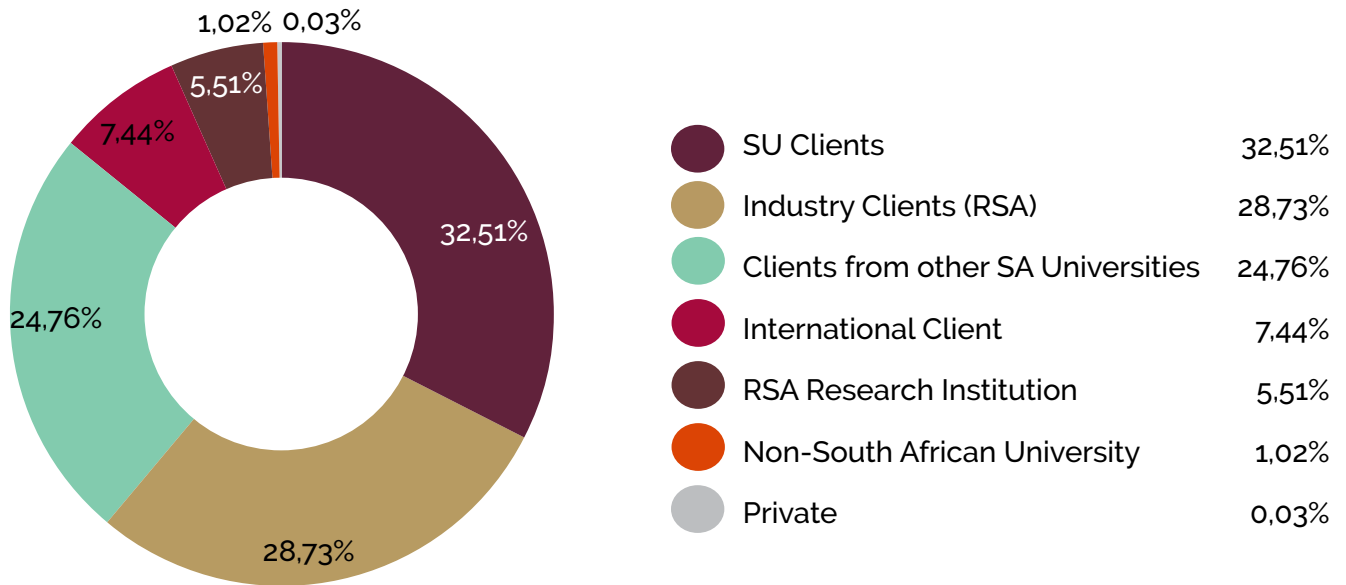
Figure 31: *Analysis of percentage of CAF income for 2021 from internal clients by faculty.*

Faculty of Science	44,14%
Faculty of Agrisciences	36,47%
Faculty of Medicine & Health Sciences	12,76%
Faculty of Engineering	6,50%
Faculty Art & Social Sciences	0,14%
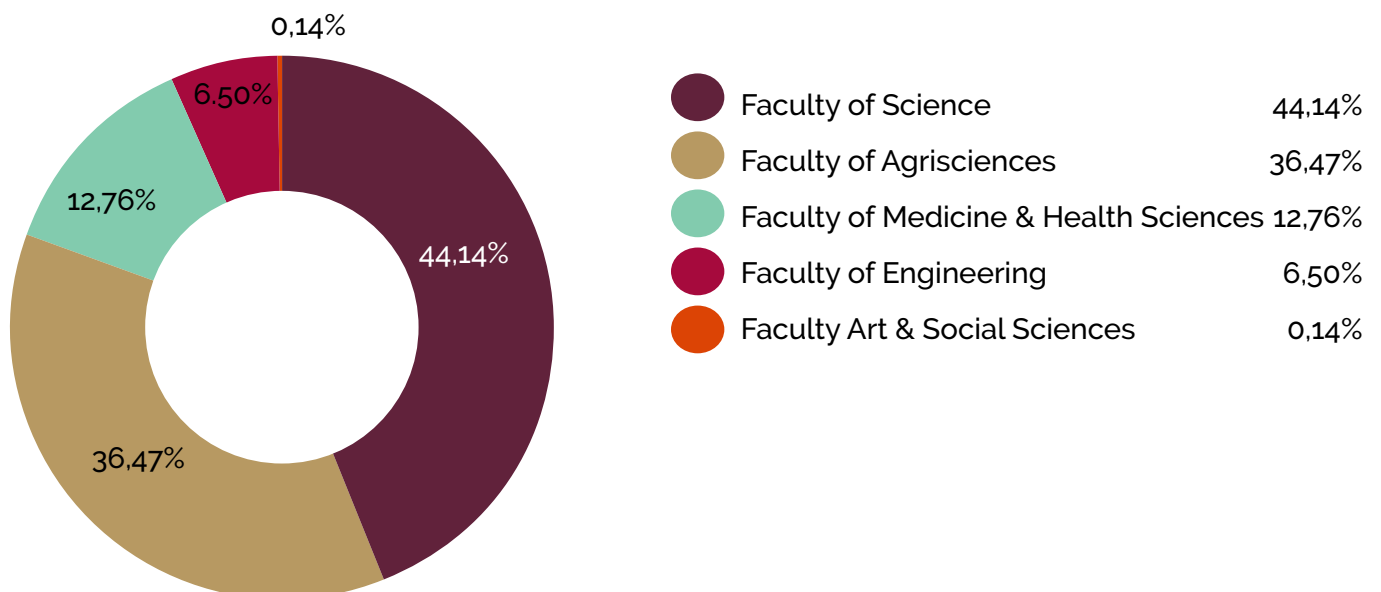
Figure 32: *Analysis of CAF income for 2021 from South African external academic clients by university.*

University	Percentage
University of Cape Town	27,35%
Cape Peninsula University Bellville	11,98%
University of Kwazulu-Natal	9,62%
University of the Western Cape	8,65%
University of Pretoria	7,61%
University of Johannesburg	6,50%
University of Venda	5,99%
Rhodes University	3,94%
University of the Free State	3,13%
University of the Witwatersrand	3,00%
Central University of Technology (Fs)	2,53%
North-West University	2,50%
Tshwane University of Technology	1,99%
Unisa	1,70%
Nelson Mandela University	1,27%

Less than 1%:

University	Percentage
Walter Sisulu University	0,69%
Durban University of Technology	0,61%
University of Fort Hare	0,42%
University of Mpumalanga	0,36%
University of Limpopo	0,12%
University of Zululand	0,05%
Vaal University of Technology	0,01%

Figure 33: *Analysis of the proportion of CAF income for 2021 from external clients.*

8,45%

91,55%

- National income 91,55%
- International income 8,45%
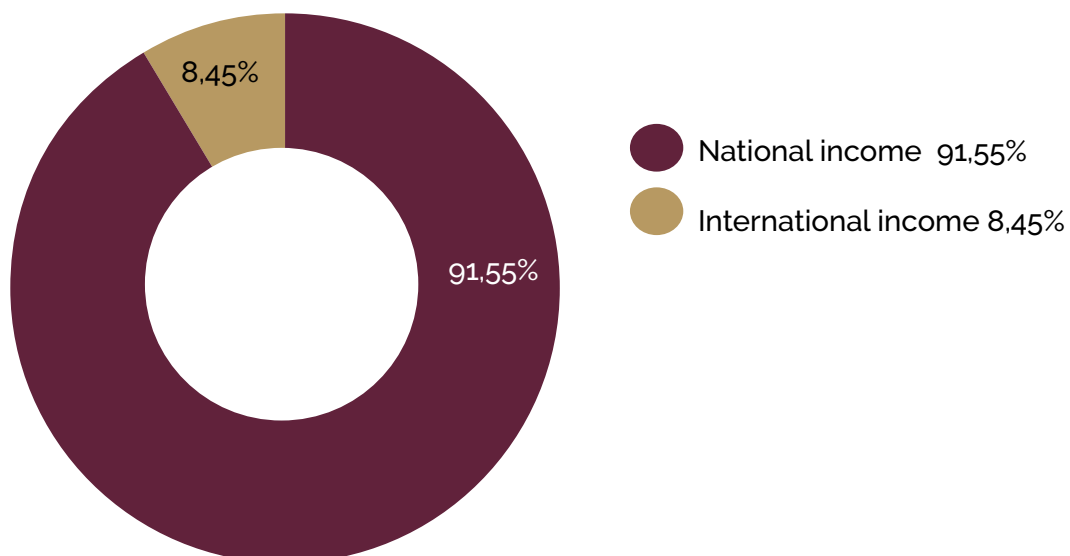
CAF structure 2022

Figure 34: *CAF structure for 2022 showing management, units and nodes.*

MANAGEMENT
Director: Prof Gary Stevens • Manager: Mrs Fransien Kamper

Mass Spectrometry Unit

Dr Marietjie Stander

GC-MS
LC-MS
Proteomics

DNA Sequencing Unit

Mr Carel van Heerden

NGS
DNA sequencing/
fragment analysis

Microscopy Unit

Vacant

Nuclear Magnetic Resonance Unit

Dr Jaco Brand

Flow Cytometry Unit

Dr Dalene de Swardt

ICP-MS & XRF Unit

Mrs Riana Rossouw

ICP-MS & XRF
Geochronology

CT Scanner Unit

Vacant

Neuromechanics Unit

Vacant

BIOGRIP Node for Soil and Water Analysis

Dr Janine Colling

NuMeRI Node for Infection Imaging (NII)

Dr Alex Doruyter

EDITORIAL TEAM

Writers:
Dr Jurgen Kriel
Lize Engelbrecht
Dr Mare Vlok
Riana Rossouw
Dr Dalene de Swardt

Compiled by:
Elbie Els

Financial Information:
Fransien Kamper

Design & Layout:
Elbie Els

Stellenbosch

UNIVERSITY
IYUNIVESITHI
UNIVERSITEIT

forward together
sonke siya phambili
saam vorentoe

CAF
Central
Analytical
Facilities

STELLENBOSCH UNIVERSITY

2021/2022 Annual Report *of the*
Central Analytical Facilities